

Search for associations containing young stars (SACY)

V. Is multiplicity universal? Tight multiple systems^{★,★★,★★★}

P. Elliott^{1,2}, A. Bayo^{1,3,4}, C. H. F. Melo¹, C. A. O. Torres⁵, M. Sterzik¹, and G. R. Quast⁵

¹ European Southern Observatory, Alonso de Cordova 3107, Vitacura Casilla 19001, Santiago 19, Chile
e-mail: pelliott@eso.org

² School of Physics, University of Exeter, Stocker Road, Exeter, EX4 4QL

³ Max Planck Institut für Astronomie, Königstuhl 17, 69117, Heidelberg, Germany

⁴ Departamento de Física y Astronomía, Facultad de Ciencias, Universidad de Valparaíso, Av. Gran Bretaña 1111, 5030 Casilla, Valparaíso, Chile

⁵ Laboratório Nacional de Astrofísica/MCT, Rua Estados Unidos 154, 37504-364 Itajubá (MG), Brazil

Received 21 March 2014 / Accepted 5 June 2014

ABSTRACT

Context. Dynamically undisrupted, young populations of stars are crucial in studying the role of multiplicity in relation to star formation. Loose nearby associations provide us with a great sample of close (<150 pc) pre-main sequence (PMS) stars across the very important age range (\approx 5–70 Myr) to conduct such research.

Aims. We characterize the short period multiplicity fraction of the search for associations containing young stars (SACY) sample, accounting for any identifiable bias in our techniques and present the role of multiplicity fractions of the SACY sample in the context of star formation.

Methods. Using the cross-correlation technique we identified double-lined and triple-lined spectroscopic systems (SB2/SB3s), in addition to this we computed radial velocity (RV) values for our subsample of SACY targets using several epochs of fiber-fed extended range optical spectrograph (FEROS) and ultraviolet and visual echelle spectrograph (UVES) data. These values were used to revise the membership of each association that was then combined with archival data to determine significant RV variations across different data epochs characteristic of multiplicity; single-lined multiple systems (SB1).

Results. We identified seven new multiple systems (SB1s: 5, SB2s: 2). We find no significant difference between the short period multiplicity fraction (F_m) of the SACY sample and that of close star-forming regions (\approx 1–2 Myr) and the field ($F_m \leq 10\%$). These are seen both as a function of age and as a function of primary mass, M_1 , in the ranges P [1:200 day] and M_2 [$0.08 M_\odot - M_1$], respectively.

Conclusions. Our results are consistent with the picture of universal star formation, when compared to the field and close star-forming regions (SFRs). We comment on the implications of the relationship between increasing multiplicity fraction with the primary mass within the close companion range in relation to star formation.

Key words. techniques: radial velocities – stars: binaries: spectroscopic – stars: formation – stars: variables: T Tauri, Herbig Ae/Be – stars: pre-main sequence – open clusters and associations: general

1. Introduction

Multiple stellar systems are abundant in our solar neighbourhood (Duquennoy & Mayor 1991; Raghavan et al. 2010) and in our galaxy; they can be found in a variety environments, from young star-forming regions (SFRs) (Ghez et al. 1997; Nguyen et al. 2012) to older, sparser populations such as globular clusters (Sollima et al. 2007). These numerous multiple systems appear to be the default of nature and therefore studying them is studying a key ingredient of star formation and evolution.

When studying the relevance of multiplicity in the context of star formation, two elements, mass and age, are key. Different masses can provide information on the formation mechanism of the stellar systems (Duquennoy & Mayor 1991; Fischer & Marcy

1992; Chini et al. 2012). The age of the system is related to the evolutionary state and history of dynamical effects (Mason et al. 1998). One must also consider the surrounding environment of the star; the density of stars increases the probability of dynamical interaction and perturbation whereby binary systems can be destroyed (Kroupa 1995; Parker et al. 2009).

The seminal work of Duquennoy & Mayor (1991) along with the more recent work of Raghavan et al. (2010) provide robust statistics of multiplicity frequency for solar-type stars in the field. Combining results from studies of higher-mass stars (Kouwenhoven et al. 2007; Chini et al. 2012) and lower-mass stars (Henry & McCarthy 1990; Fischer & Marcy 1992) the multiplicity frequency can be shown as a function of mass, as seen in Figure 12 of Raghavan et al. (2010). The field stars used in such studies have been dynamically processed in different ways (Parker et al. 2009). In contrast, stars in associations are considered coeval with low average stellar densities and are much younger \sim 1–100 Myr. We can therefore use these populations of stars as samples from which the effects of dynamical processing are very small and the observables are much closer to the direct outcome of star formation.

* Based on observations obtained using the instruments FEROS at La Silla (ESO 1.5m and MPG/ESO 2.2m) UVES at VLT (ESO 8m)

** Appendices C and D are available in electronic form at

<http://www.aanda.org>

*** Tables C.1, C.2, and D.1 are available in electronic form at the CDS via anonymous ftp to cdsarc.u-strasbg.fr/130.79.128.5 or via <http://cdsarc.u-strasbg.fr/viz-bin/qcat?J/A+A/568/A26>

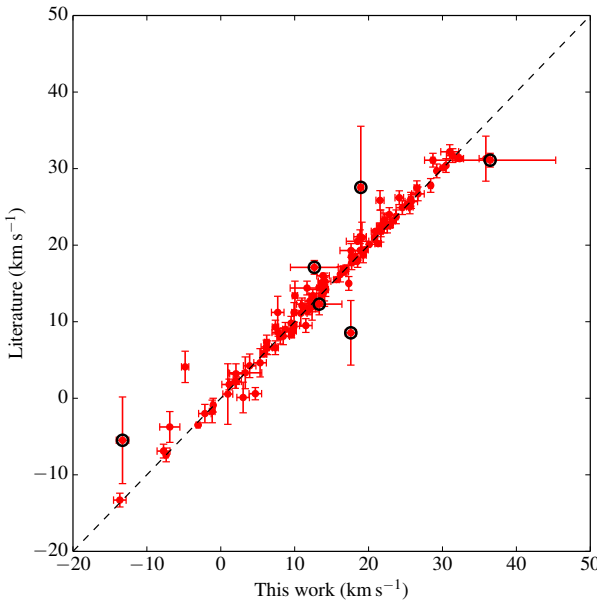


Fig. 1. Average RV values determined in this work versus those from the literature, where values were available for comparison. Error bars represent the standard deviation from the mean value for each source. If uncertainties were not quoted in the literature, the average uncertainty from all other values, 0.90 km s^{-1} , was used. If only one data epoch was available, the overall standard deviation for the SACY sample, 0.89 km s^{-1} , derived in this work was used to represent the uncertainty. Black rings indicate identified multiple systems. A line representing a 1:1 relation has been drawn for base comparison.

The coeval populations that are usually studied comprise young nearby SFRs (1-5 Myr), such as Taurus-Auriga, Ophiuchus-Scorpius, and Chamaeleon (Melo 2003; Ghez et al. 1993; King et al. 2012b), across a wide range of orbital periods ($\sim 1\text{-}1000 \text{ A.U.}$). The results from these environments are difficult to compare due to variable extinction properties and large distances ($\geq 135 \text{ pc}$). However, some studies aim to do this (King et al. 2012b,a) using the limited overlapping parameter space between populations to produce robust multiplicity statistics.

In addition to SFRs, close associations, which are loose collections of stars sharing common kinematics, can offer populations that are close enough to the Sun to probe a large and continuous range of orbital periods. They also provide targets to study the transitional phase of disk dispersal. The search for associations containing young stars (SACY) sample is comprised of nine close associations, as detailed in Table D.1, with ages of $\sim 5\text{-}70 \text{ Myr}$ and distances of $< 150 \text{ pc}$ (Torres et al. 2006, 2008). This paper is part of a series studying the SACY associations, concentrating on their multiplicity properties relating to star formation and disk evolution. The multiplicity results presented in this paper are derived spectroscopically, probing the short period systems of the SACY sample and are compared to other populations, such as young close SFRs and the field.

The paper is organised as follows. Section 2 details the observations and data used in this work. Section 3 describes the use of new radial velocity (RV) data to determine association membership and details the estimation of the mass distribution of the observed sample. Section 4 describes the methods employed to find multiple systems within our sample and the methods to account for biases. Section 5 presents the results and their

Table 1. Summary of the properties of SACY associations studied in this work. The age uncertainties provided represent the dispersion found in the literature. This dispersion is large; however, the relative aging performed with Li should not be affected.

Association	Ass. ID	Dist. (pc)	Age (Myr)	+ / - (Myr)	N. of Obj.	N. of SBs
AB Doradus	ABD	34 ± 26	70	30 / 20	53	5
Argus	ARG	106 ± 51	40	10 / 30	33	0
β -Pic	BPC	31 ± 21	10	10 / 8	29	4
Carina	CAR	85 ± 35	30	5 / 20	22	3
Columba	COL	82 ± 30	30	40 / 15	31	1
ϵ -Cha	ECH	108 ± 9	6	1 / 0	20	2
Octans	OCT	141 ± 34	20	10 / 10	13	1
Tuc-Hor	THA	48 ± 7	30	0 / 20	33	0
TW-Hydrae	TWA	48 ± 13	8	2 / 3	11	0

significance in relation to star formation. Finally in Section 6 the conclusions of this work on multiplicity and future prospects are presented. Appendix A shows the spectral type to effective temperature conversion. Appendix B notes individual sources; Appendix C details of the individual RV values, and Appendix D the targets considered as members in the SACY sample.

2. Observations and data

There are two main sources of high resolution spectroscopy available to us.

First, observations performed with the fiber-fed extended range optical spectrograph (FEROS), a high resolution echelle spectrograph ($\lambda/\Delta\lambda \sim 50,000$) at La Silla, Chile in two distinct periods: between January 1999 and September 2002 at the 1.5m/ESO telescope (ESO program ID: 67.C-0123) and after October 2002 at the 2.2m telescope (ESO program IDs: 072.C-0393, 077.C-0138). These data were reduced and RV values were calculated for these targets as described in Torres et al. (2006). Out of the total SACY sample used in this work, 127 sources have existing RV values from FEROS data and multiplicity flags.

Second, observations performed with the ultraviolet and visual echelle spectrograph (UVES) ($\lambda/\Delta\lambda \sim 40,000$ with $1''$ slit) at Paranal, Chile with ESO program IDs: 088.C-0506(A) & 089.C-0207(A) between October 2011 and September 2012. In these two programs each source had three separate observations using the standard set-up, a $1''$ slit width, which covers the wavelength range $3250\text{-}6800 \text{ \AA}$. The separation in time between the acquisition of each epoch of data for one source ranges from 1 day to ~ 1 month; the simulations described in Section 4.2 help to characterize possible bias from this time sampling.

In addition, for each source, the UVES archive was queried to make use of all available and public data on the SACY targets. All data were reduced using the UVES pipeline recipe *uvess_obs_redchain* with the command-line driven utility *esorex* (bias corrected, dark current corrected, flat-fielded, wavelength-calibrated and extracted). This outputs three individual spectra, (in the case of the standard set-up) one spectrum for each CCD chip of the instrument: blue, red upper and red lower (BLUE $3250\text{-}4500 \text{ \AA}$, REDU $4800\text{-}5800 \text{ \AA}$, and REDL $5800\text{-}6800 \text{ \AA}$,

respectively).

In addition, the VizieR catalogue service was used to look for any existing RV values. A comparison between the archival data and the SACY values is shown in Figure 1. The individual values from UVES, FEROS and archival sources is shown in Table C.1 with their respective uncertainties; the average uncertainty from the literature is 0.9 km s^{-1} .

3. Characterising the sample

3.1. Revising membership with new RV data

Accurately determined RV values are a key ingredient to the convergence method (Torres et al. 2006) used to identify the SACY association members. The convergence method uses the gamma (systemic) velocity; in the case of single stars, this is equal to the RV. For multiple systems without orbital solutions, there are two cases, with multi-component spectra (SB2/SB3) and without (SB1). For SB2/SB3 systems it is derived from weighting the component RV values, according to their relative flux. For SB1 systems the mean RV value is used with its respective variability induced by further components (certainty of membership for these systems is very difficult without an orbital solution). For multiple systems with orbital solutions it is a known value. Therefore the more accurate the RV values and, in the case of multiple systems, the greater phase coverage observed, the more stringent the conditions for membership become.

The large number of RV values calculated in this work was used to revise and refine the member list (da Silva et al. 2009). With this new data any targets that no longer had a high probability of membership were removed from the overall analysis and statistics of the associations (initial members and revised members are shown in Table D.1). However, as we have conducted useful analysis on these objects, details can be found in Appendix B.

3.2. Mass distribution

The mass distribution was constructed using effective temperatures from da Silva et al. (2009). First, available effective temperature were used directly with age estimates, as given in Torres et al. (2006), to obtain a model-based mass using isochrones (Baraffe et al. 1998, 2003; Siess et al. 2000). The different isochrones were used depending on the temperature range. The median effective temperature for each spectral subclass within each association was used to estimate a value for those targets with a spectral type, as calculated by the method described in Torres et al. (2006), but without an effective temperature value. Linear interpolation was used for those spectral subclasses without any corresponding temperature values from da Silva et al. (2009). In the case of Carina (CAR), effective temperature values for targets of spectral type K3 and later were taken from median values of Tucana-Horologium (THA), which are approximately the same age, and having a much larger population in this spectral type range. Masses were then derived using effective temperatures and isochrones to produce a mass distribution, as shown in Figure 2.

To validate this method we derived masses from a calculated bolometric luminosity value using the VOSA tool (Bayo et al. 2008) by assuming a solar metallicity (Viana Almeida et al. 2009) and $\log(g)$ between 3.5 and 5. This value is calculated from a fit of the Spectral Energy Distribution (SED). Some 78 sources had poor SED fits due to a lack of available

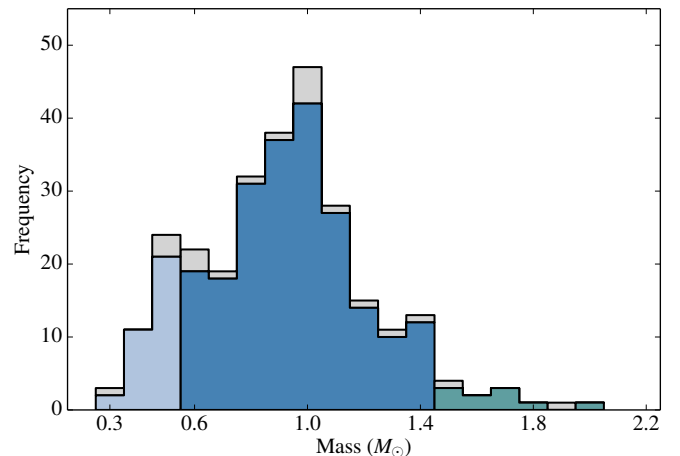


Fig. 2. Mass distribution of all targets used in this work calculated by using available effective temperatures from da Silva et al. (2009) and derived masses using Baraffe et al. (2003) models $< 0.6 M_\odot$ – light blue, Baraffe et al. (1998) models between masses $0.6\text{--}1.4 M_\odot$ – dark blue, and Siess et al. (2000) models $> 1.4 M_\odot$ – green. The grey represents multiple system primary masses.

photometry and therefore could not be used any further. The calibration of the bolometric luminosity is also based on the distance, which is the largest source of uncertainty. This uncertainty combined with the photometric error count yields a further 65 sources (from ≈ 250) with an error in bolometric luminosity $> 20\%$ of the calculated value. For the remaining sources, we derived the masses with the bolometric luminosity value using the isochrones. The standard deviation in masses derived from the two different methods was $0.07 M_\odot$. This is a very small and acceptable difference in our model-based masses.

The mass distribution calculated from the effective temperatures was used in this work, as opposed to that calculated from the bolometric luminosity, as it represents our sample more fully.

4. Identifying multiple systems

To determine the RV values, we computed cross-correlation functions (CCFs) for all reduced spectra with a signal-to-noise ratio greater than 10. To compute the CCF, the observed spectrum is convolved with a CORAVEL-type numerical mask, as described in Queloz (1995). The shape of the CCF function is approximated by a Gaussian profile and, in cases of fast rotation, the Gray rotational profile (Gray 1976). The RV is the peak of this profile to which the barycentric correction is applied.

For the sake of homogeneity, all CCFs quoted in this paper have been calculated using a K0 mask, including those without a literature spectral type determination. Double-lined spectroscopic systems (SB2s) – and in rare cases, triple-lined spectroscopic system (SB3s) – are identified visually, displaying two distinct peaks in the outputted CCF. For systems with indications of multiplicity in the CCF profiles, such as two apparently merged components, more research and analysis was conducted, the details of which can be found in Appendix B.4. Examples of the CCF output for these systems and that of a system with no indication of multiplicity are shown in Figure 3.

Single-lined spectroscopic systems (SB1s) are identified through significant RV variations between different data epochs; the results are shown in Figure 4. The shaded area contains all

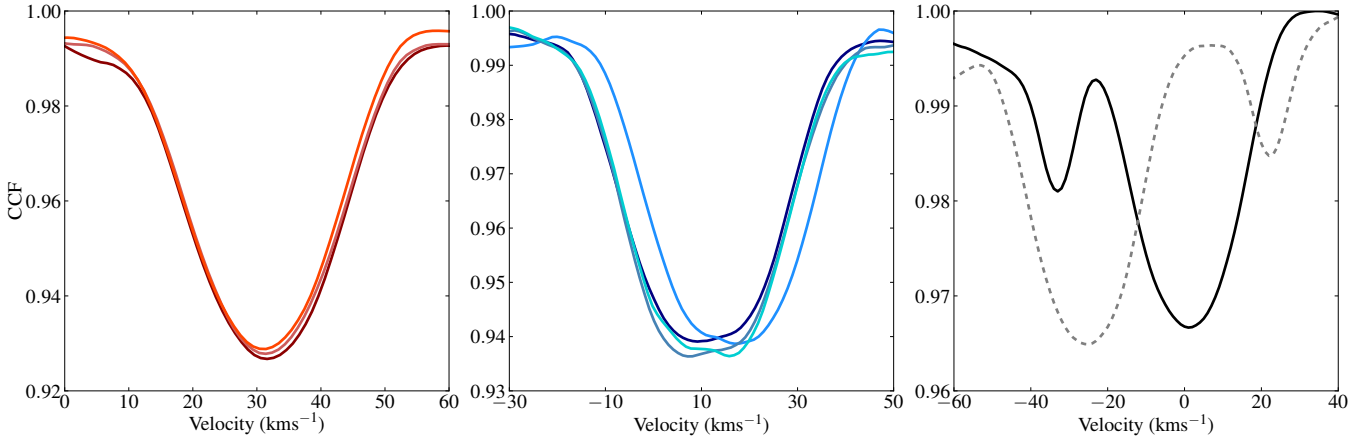


Fig. 3. Resulting CCF profiles from three different sources. *Left Panel:* HD 45270 with no significant variation in RV and standard deviation $< 0.05 \text{ km s}^{-1}$ (data epochs: 2007-05-08, 2008-12-05, 2010-09-26). *Central Panel:* HD 104467 a SB1 candidate with significant variation in RV and std dev. $> 2.70 \text{ km s}^{-1}$ (data epochs: 2009-03-16, 2010-05-26, 2012-02-24, 2012-03-07). *Right Panel:* HD 155177 a SB2 system, as shown by two clear peaks and temporal movement (data epochs: 2007-04-19, 2012-05-09).

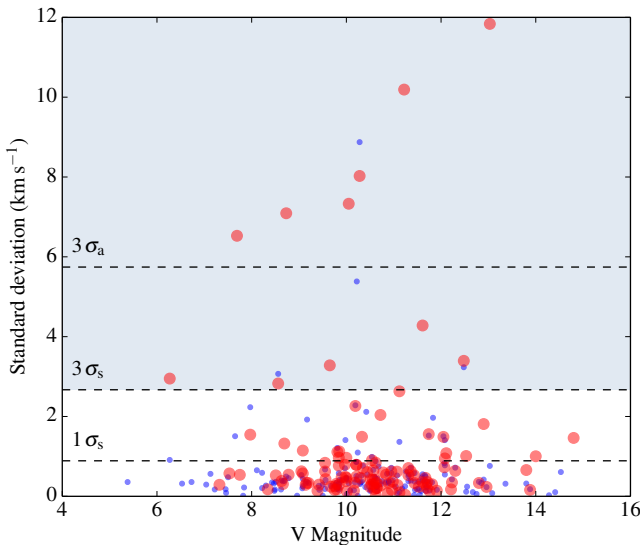


Fig. 4. The standard deviation in RV values for SACY sources, excluding known SB2 systems, as a function of V magnitude. UVES and FEROS values – blue dots and UVES, FEROS and archival data – red circles. The variables, $1\sigma_s$ and $3\sigma_s$, represent one standard deviation and three standard deviations respectively, for both UVES and FEROS data. The shaded area contains SB1 candidate multiple systems. The variable $3\sigma_a$, represents three standard deviations including archival data.

the SB1 candidates; these candidates have significant RV variations; above $3\sigma_s$ (2.70 km s^{-1}), or three standard deviations for the entire dataset. The value of three standard deviations, $3\sigma_a$, including archival data is also shown for comparison. All candidates above $3\sigma_s$ were investigated further, details can be found in Appendix B.1.

4.1. Sources of uncertainty

The uncertainty in the RV values is calculated from equation (9) of Baranne et al. (1996):

$$\sigma_{\text{meas.}} = \frac{C(T_{\text{eff}})}{D \times S/N} \frac{(1 + 0.2\omega)}{3} \text{ km s}^{-1}, \quad (1)$$

where $C(T_{\text{eff}})$ is a constant that depends on both the spectral type of the star and the mask used, which is typically 0.04, ω is the (noiseless) FWHM (km s^{-1}) of the CCF, D is its (noiseless) relative depth, and S/N is the mean signal-to-noise ratio.

This produces a value, which is the internal uncertainty for the measurement of the RV using this CCF method. Due to the very high signal-to-noise ratio in our data (average ~ 100), the contribution of this internal uncertainty is almost negligible. Although the value of $C(T_{\text{eff}})$ is a function of the T_{eff} and the mask used to compute the variation in the temperature range 4000–6000 K, it only changes the value of $C(T_{\text{eff}})$ by ≈ 0.01 . When this variation is propagated across the T_{eff} , the output range is not significantly affected. Values are $\sim 0.01 \text{ km s}^{-1}$. However, the stars in our study are often variable, and this can induce deformities into the CCF (Lagrange et al. 2013) in which this calculation of uncertainty does not account for; it assumes a symmetric CCF profile, and thus, the uncertainty is underestimated in the majority of cases.

A more empirical approach to gauging the level of uncertainty in the measurements is to use the standard deviation of the RV values, as shown in Figure 4. This is an *a posteriori* approach, assuming a very small percentage of our candidates are in multiple systems, and that this overall distribution is mainly representing single systems. Previous research in SFRs concerning short period multiplicity of T-Tauri stars has shown that single systems are by far the most abundant 90% (Melo 2003) and have used such distributions to estimate empirical uncertainties. The one sigma level in RV variation for all targets with more than one data epoch (excluding known SB2 systems) is 0.89 km s^{-1} , as seen in Figure 4.

4.2. Accounting for biases

A huge advantage of the SACY dataset is the way in which the sample was compiled from optical counterparts to X-ray sources from the ROSAT all-sky survey. X-ray emission can originate in protostars $\sim 10^4 - 10^5$ yr (Koyama et al. 1996) to post T-Tauri stars ~ 10 Myr (Walter et al. 1988). In terms of mass this is from sub-stellar (Neuhäuser et al. 1999) to intermediate-mass Herbig Ae/Be stars (Zinnecker & Preibisch 1994). On this basis, our sample should be relatively free of significant bias for ages and

primary masses (\sim 5-70 Myr and 0.5-3.0 M_{\odot}). However, the sample is not bias-free regarding the characteristics of the secondary components and orbital parameters.

To estimate the completeness of this work, given the sparse and irregular time sampling, in terms of our sensitivity in observing binary systems, probability-detection density maps were created using a set of synthetic binary systems, as described in Section 6.1 of Duquennoy & Mayor (1991) and outlined further below. The primary masses used in these simulations are the mean values of mass bins containing equal numbers of targets (0.6, 0.9 and 1.2 M_{\odot} : 85 targets) taken from the overall mass distribution of the sample, which includes all targets with cross-correlation results not previously identified as SB2 systems.

For each primary mass, a density map as a function of the secondary mass (M_2) and the period (P) of the binary system was constructed. A set of binary systems are generated in this space (M_2/M_1 : 0.1 M_{\odot} to M_1 , P : 1 to 1000 day) following certain distributions. The parameters phase at time $t=0$ ($\phi_{t=0}$), longitude of the ascending node (ω) and the inclination (i), are randomly drawn from uniform distributions within their respective numerical ranges. The eccentricity (e) values depend on the period of the binary system as follows:

- $P < 8$ day, $e \equiv 0$
- $P \leq 8 < 1000$ day, e is randomly drawn from a normal distribution centred at 0.33 with a standard deviation of 0.03 (Mayor & Mermilliod 1984).

The semi-amplitude (K) and thus the RV were then calculated through equations (14) and (17) from Halbwachs (2001) using our physical set of data epochs to input the time (t) into the equations. For each object, a set of RVs is produced, and from this, the standard deviation from the mean is calculated. If this calculated value is above the standard deviation of our physical, observed data the system is said to be *observed*; this process is then repeated N times for each (M_2, P) point.

For this range Figure 5 shows that the effect of the primary mass of the binary system has little effect on the sensitivity to observe the secondary. For all three primary masses considering a secondary component of 0.1 M_{\odot} , orbital periods of 30 day and 100 day have a $>75\%$ and $>60\%$ probability, respectively, of being detected within our dataset.

5. Results and discussion

The individual targets classified as multiple systems are shown in Table 2, which are identified either as SB1, SB2 or SB3. We then calculate the multiplicity fraction (F_m):

$$F_m = \frac{B + T + Q}{S + B + T + Q}, \quad (2)$$

where S , B , T , and Q are the number of single, binary, triple, and quadruple systems, respectively.

We use the multiplicity fraction, as opposed to the Companion Star Fraction (CSF), which is the number of companions per star, because the multiplicity fraction is more robust against unobserved higher order components (Hubber & Whitworth 2005), whether a multiple system is a binary or a triple system the overall value of F_m would not be affected.

5.0.1. Multiplicity fraction as a function of age

The SACY sample has age determinations calculated in Torres et al. (2008). However, there are significant uncertainties within

Table 2. Targets classified as multiple systems.

ID	Mass (M_{\odot})	SpT	Ass.	Age (Myr)	Flag
GSC 09420-00948	0.6	M0	ECH	6	SB1 ^a
HD 104467	1.9	G3	ECH	6	SB1 ^a
V1005 Ori	0.7	M0	BPC	10	SB1 ^b
HD 59169	1.05	G7	ABD	70	SB1 ^a
PX Vir	0.9	K1	ABD	70	SB1 ^b
CD-2711535	1.0	K5	BPC	10	SB1 ^{a,b}
AK Pic	1.2	G2	ABD	70	SB1 ^b
GSC 08077-01788	0.6	M0	COL	30	SB1 ^{a,b}
1RXS J195602.8-320720	0.3	M4	BPC	10	SB2 ^a
V4046-Sgr	1.1	K6	BPC	10	SB2
HD 155177	1.5	F5	OCT	20	SB2 ^a
BD-20951	1.0	K1	CAR	30	SB2
HD 309751	1.05	G5	CAR	30	SB2
TWA 20*	0.4	M3	TWA	8	SB2
CD-423328	1.0	K1	CAR	30	SB2 ^{b,c}
HD 217379	0.6	K7	ABD	70	SB3
HD 33999	1.3	F8	ABD	70	SB3

Notes. (*) No longer classified as a member of TWA with new RV data. (a) System has not been previously identified in related SACY work or literature. (b) Targets classified based on variation from literature RV values. (c) Details of the technique to classify this target are described in section B.4.

these determinations (as shown in Table 1), which are derived using a convergence method represented by third degree polynomials of $(V - I)_C$. There is an abundance of papers on the age determination of young associations, including the well-known β -Pic: 12^{+8}_{-4} Myr (Zuckerman et al. 2001), 20 ± 10 Myr (Barrado y Navascués et al. 1999), TW-Hydrae: 10^{+10}_{-7} Myr (Barrado y Navascués 2006). This is often a controversial subject; however, the relative ages between the associations are less affected and, therefore, are more robust quantities. In other words, it is known that TW-Hydrae is younger than Tucana-Horologium, irrespective of their absolute ages, as seen in da Silva et al. (2009), Figure 3.

If there was a significant relationship between multiplicity and age (between ages \sim 5-70 Myr) we could observe it. However, as shown in Figure 6, we see no such trend, merely scatter across the age range. These results also agree with data from Young clusters, Tau-Aur and Cha I with ages 1 Myr and 2 Myr, respectively (Luhman 2004). In addition to this when considering results from the field within the orbital period range (1-200 day), the fraction, $0.073^{+0.014}_{-0.012}$, is indistinguishable (Duquennoy & Mayor 1991; Nguyen et al. 2012).

These results can be explained by the minimal N-body dynamical processing for systems with small physical separations (< 50 A.U.). Such systems are essentially never destroyed (Parker et al. 2009), and if we assume similar numbers of multiple systems are created from population to population initially, we would not expect to see a significant relationship with time.

5.0.2. Multiplicity fraction as a function of mass ($< 3M_{\odot}$)

To compare our results in terms of primary mass to previous work, we must define a consistent period and secondary mass range and apply the same correctional techniques. Nguyen et al. (2012) studied the range $P_{\min}=1$, $P_{\max}=200$ day and $M_{2,\min}=0.08$, $M_{2,\max}=0.6 M_{\odot}$. The properties of the synthetic bi-

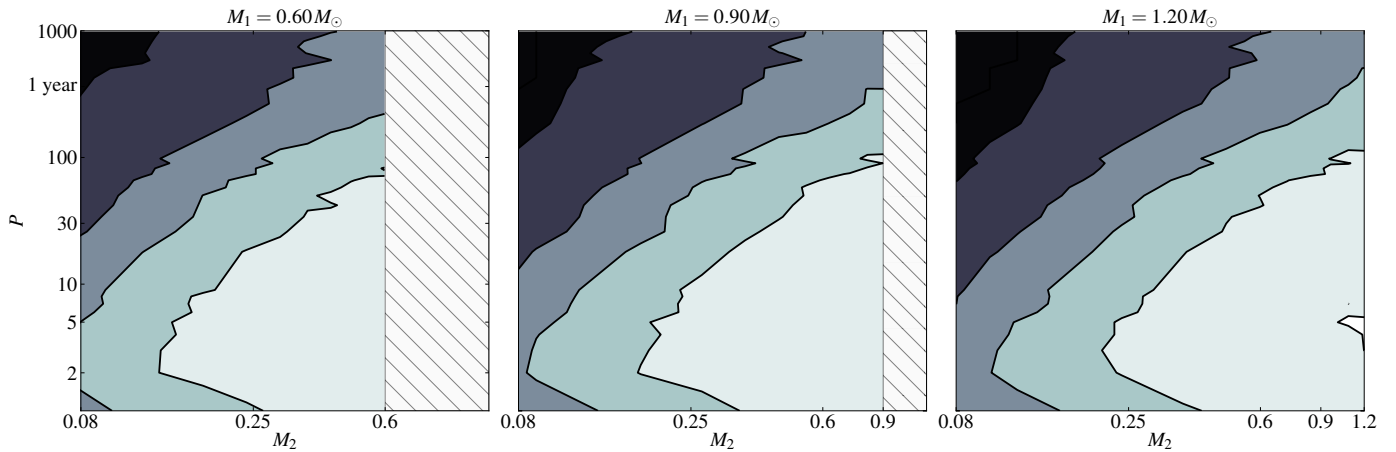


Fig. 5. Probability density maps in (M_2, P) space for three different primary mass stars, $0.60, 0.90$, and $1.20 M_{\odot}$, periods, P , range from 1–1000 day, and secondary masses, M_2 , from $0.1 M_1 - M_1$. Probabilities: $< 5\%$ – black, $5\text{--}39\%$, $40\text{--}59\%$, $60\text{--}74\%$, $75\text{--}90\%$ and $> 90\%$ – white.

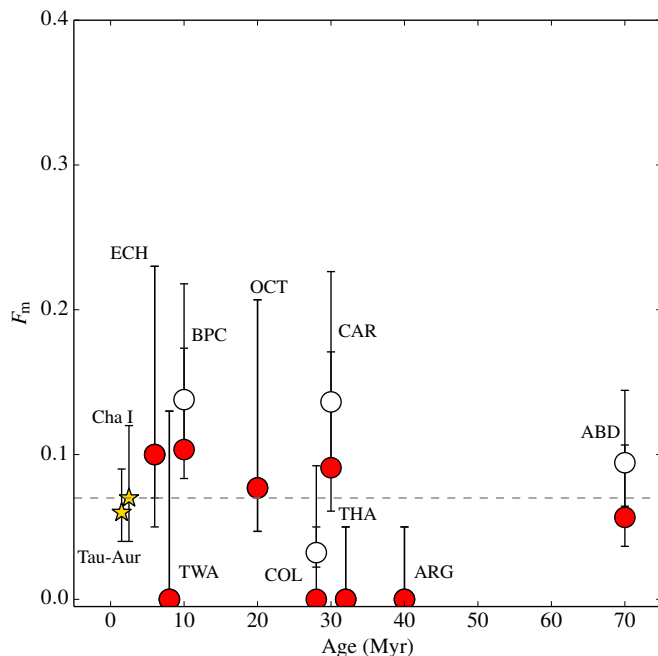


Fig. 6. The fraction of spectroscopic multiple systems from the overall observed sample as a function of age for each of the SACY associations, which are individually labelled. UVES and FEROS data – red, UVES, FEROS and archival data – white, and data from Nguyen et al. (2012) – yellow. Uncertainties were derived from low-number statistics using Equation (A3) from Burgasser et al. (2003). A line representing 7% multiplicity is shown.

naries used in their simulations are taken from a typical T-Tauri star in their sample; however we have calculated detection probabilities using three primary masses ($0.6, 0.9$ and $1.2 M_{\odot}$) in this work.

We can estimate the probability that the multiple system will be in this P and M_2 range from each primary mass M_1 using Bayes' theorem (Bayes & Price 1763):

$$\mathcal{P}_{M_1}(m, p) = \frac{\sum_{m=M_2,\min}^{M_2,\max} \sum_{p=P_{\min}}^{P_{\max}} \mathcal{M}(m, p) \mathcal{D}(m, p)}{\sum_m \sum_p \mathcal{M}(m, p) \mathcal{D}(m, p)}, \quad (3)$$

where $\mathcal{M}(m, p)$ is the prior distribution. In this case the most ignorant prior distribution is used, $\mathcal{M}(m, p) = 1$, and $\mathcal{D}(m, p)$ is the likelihood function from our probability of detection simulations.

We compute the probability for each of our primary masses and use the mean detectability probability to compute a corrected fraction, as below:

$$F_{\text{correc}} = \frac{F_{\text{obs}} \times \mathcal{P}_{M_1}(m, p)}{\frac{1}{N} \sum_{m=M_2,\min}^{M_2,\max} \sum_{p=P_{\min}}^{P_{\max}} \mathcal{D}(m, p)}, \quad (4)$$

where F_{correc} is the corrected fraction, F_{obs} is the observed fraction, and N is the number of separate detection probabilities from the simulations.

The results of these corrected fractions are shown in Figure 7, along with data from Nguyen et al. (2012). Our mass bins contain equal numbers of targets (85) to eliminate any bias from the frequency of objects in a certain mass range. The results are fully compatible, and the spread in the value of F_{correc} including the uncertainties is only 7% across the mass range ($\approx 0.2\text{--}2.0 M_{\odot}$). This result also supports the universality of multiplicity, as the data from the two different environments (loose associations and denser SFRs) is indistinguishable.

As well as comparing the results from SACY to those of younger SFRs, one can look at the form of the corrected fraction with primary mass for both environments. Figure 7 shows there is no significant increase or decrease in the corrected fraction as a function of the primary mass. In other words, from our results, it is just as likely to observe a multiple system with a primary mass of $\approx 0.2 M_{\odot}$ than one with a primary mass of $\approx 2.0 M_{\odot}$. As shown and discussed in Section 5.0.3 when higher masses are included the form changes quite dramatically.

5.0.3. Multiplicity fraction across a wide mass range

There are two phases of interaction that can shape the multiplicity fraction we observe in populations of stars: (I.) Interactions within the pre-stellar cores ($\leq 10^5$ yr) through accretion, disk

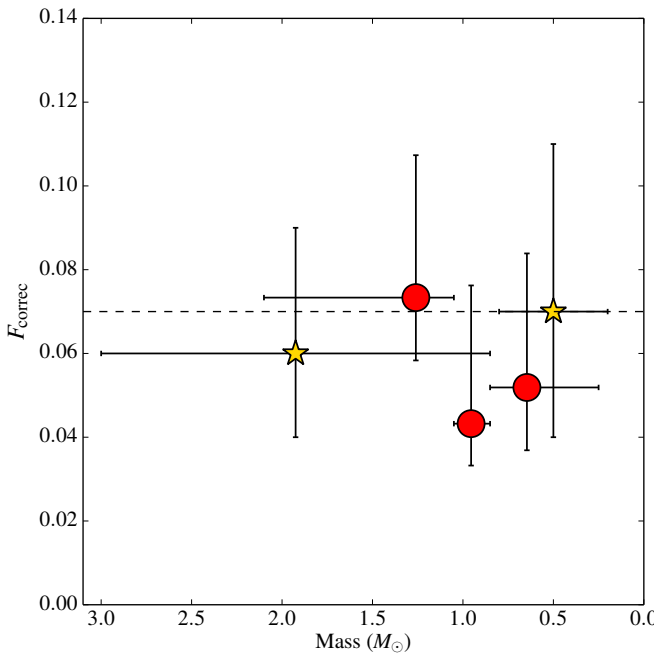


Fig. 7. Multiplicity fraction as a function of primary mass; mass bins are represented with x-axis error bars with the average value for the SACY targets being the red markers. Fractions have been corrected using the techniques outlined in Section 5.0.2. The same data (Nguyen et al. 2012) shown in Figure 6 has been transformed from spectral type to mass by assuming an age of 1 Myr and 2 Myr for Tau-Aur and Cha I respectively, using T_{eff} from Luhman (2004) and Sestito et al. (2008) with isochrones explained in Figure 2.

interaction and the dynamics of multiple systems (Bate et al. 2002) and (II.) through cluster dynamics, where the interactions between stars that have originated in different pre-stellar cores ($> 10^5$ yr), which can be modelled using N-body simulations (Kroupa 1995).

Populations that are \sim Myr have undergone significant evolution of their parameters already (e.g., mass ratio, separation distribution, and core multiplicity fraction). However, the close systems observed in this study (< 10 A.U.) should not have undergone any significant processing through the second phase described above. Therefore, even across a wide range of ages and environments, we should be probing the multiplicity fraction that is a direct result from the evolution within the separate pre-stellar cores.

Figure 8 shows a compilation of results from this study (in red and white) and from the literature (in blue and gold) for spectroscopic multiplicity fractions from a range of sources. The apparent exponential form of this function should be considered with caution in this instance, as this compilation lacks thorough refinement, such as a defined consistent orbital period range. It is a qualitative example of the trend of increasing multiplicity fraction with spectral type, and therefore mass, for tightly bound multiple systems. This trend seems to be preserved when considering much wider systems in the field, as seen in Figure 12 of Raghavan et al. (2010).

One potential explanation for this observed relationship in the field relates to the binding energy of the system; however, we would not see a significant relationship for tight binaries on this basis, (Parker et al. (2009), Section 5.2, interaction time-scale

calculations: Nguyen et al. (2012)). As shown in Figure 8, there is an increase with mass for these close systems, this is not easily explained with our current understanding of star formation.

The observed physical separation of close systems (< 10 A.U.) is the result of the evolution of the multiple system's properties. The size of the first Larson core, a pressure-supported fragment of ≈ 5 A.U. (Larson 1969), does not permit a secondary component to orbit at such a physical separation initially. Bate et al. (2002) shows how these close systems can be formed from wider systems through the processes associated with phase I with dynamical interactions being the dominant mechanism. Kozai cycles with tidal friction (KCTF) (Eggleton & Kisselava-Eggleton 2006) is an example of such a dynamical process. This evolution depends on the periods of the primary and tertiary components $P_3(P_3/P_1)$. Given $P_1 = 1$ yr and $P_3 = 1000$ yr, the time-scale for one cycle is $\sim 10^6$ yr; $> 10^2$ cycles are needed to complete the evolution (Tokovinin et al. 2006). Therefore, one could argue that this evolution is negligible at the PMS stage. However, the periods within the system could be initially much more similar and thus the ratio would be smaller, decreasing the time-scale. On this basis, this mechanism could have an effect even at the PMS stage, producing SB systems.

Bate et al. (2002) conclude that the processes described in phase I favour the production of higher mass multiple systems, which would explain the trend shown in Figure 8. If these processes are responsible for the systems we observe, there would be other related properties, such as a lack of extreme mass-ratios of the systems and a tendency for wider companions. Both of these properties will be investigated in further SACY work: Mass ratios by following up identified spectroscopic candidates to characterize their orbital parameters and wider companions by analysis and inclusion of already existing adaptive optics (AO)-assisted direct imaging data.

One must also consider the possibility that star formation is not a single universal process. King et al. (2012a) have found significant statistical differences¹ in the multiplicity fraction for binary systems in the 19–100 A.U. range (dynamically unprocessed) between the field and five clusters (Taurus, Upper Scorpius, Corona Australis, Chamaeleon I, and Ophiuchus). They conclude that the star formation process is non-universal and different environments produce different numbers of binaries due to this.

In our data presented in Figure 6, we find three associations that show no spectroscopic systems from our current dataset: Argus: 0 / 33 ($0^{+7}\%$), Tucana-Horologium: 0 / 33 ($0^{+5}\%$), and TW-Hydrae: 0 / 11 ($0^{+13}\%$). With our current dataset this means that Argus, Tuc-Hor, and TW-Hydrae have upper limits on the F_m value of 0.07, 0.05, and 0.13, respectively. These results could also be explained by the non-universality of formation; however, these are still very low numbers and are not statistically significant.

There is an alternative theory to explain this apparent spread in binary fractions (and properties): turbulent fragmentation. Jumper & Fisher (2013) describe how binary properties can be determined very early on by turbulence within the pre-stellar cores; this extremely stochastic process intrinsically leads to a range of binary properties and as a product to the formation of the Brown Dwarf (BD) desert. Therefore, one should be careful when considering multiplicity fractions as a direct key to star formation, as we still need to clarify the picture further at the early stages of formation. Work is ongoing in this area.

¹ see Marks et al. (2014) for an alternative interpretation

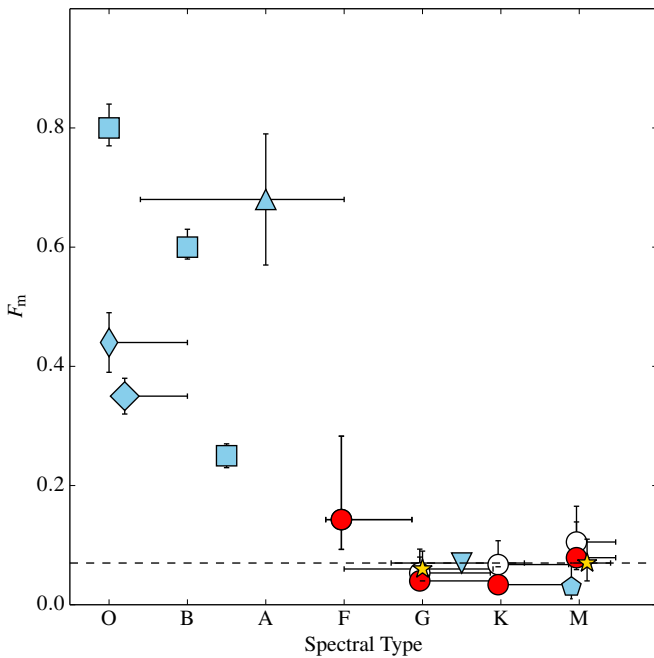


Fig. 8. The spectral type versus the multiplicity fraction for all available SACY data and studies from the literature; the horizontal error bars represent the width of the spectral class bin (symbols in red, white and yellow as described in previous figures). Chini et al. (2012) – filled square, Baines et al. (2006) – filled triangle, Sana & Evans (2011) – filled thin diamond, Sana et al. (2013) – filled diamond, Raghavan et al. (2010) – inverted filled triangle, and Fischer & Marcy (1992) – filled pentagon.

6. Conclusions and further work

1. Using our new RV determinations, we have revised the membership of the SACY associations.
2. We have identified seven new multiple systems (SB1s: 5, SB2s: 2) within the SACY sample, as shown in Table 2.
3. Within the nine SACY associations studied in this work, we have found that there is no significant age dependence on the observed fraction of spectroscopic multiple systems (F_m).
4. The corrected fraction of spectroscopic multiple systems (F_{correc}) within the mass range $\approx 0.2\text{--}2.0 M_\odot$ is compatible with a flat distribution.
5. Our results are consistent, considering fractions as a function of mass and age, with nearby SFRs and the field, as expected from the picture of universal star formation.
6. The observed fraction of spectroscopic multiple systems sharply declines as a function of spectral type and appears to plateau for later-types. To what spectral types this flat distribution extends still needs to be explored.

This study has analysed the fraction of close multiple systems through spectroscopic techniques. In the future, these results will be complimented with AO-assisted direct imaging from high-angular resolution data. Combining the analysis presented in this paper with that of much wider companions, we can get a wealth of extremely valuable information about the multiple systems in these young close loose associations and their similarities / differences to other environments in the context of star formation. We can investigate certain multiple star formation scenarios by the detection / non-detection of

wider tertiary components to the SB candidates proposed in this paper. In addition to this, we will follow up our spectroscopic candidates identified in this study to better characterize their properties such as orbital period and mass ratio.

We have analysed ≈ 2700 spectra with an average S/N of 100 and succeeded in detecting new spectroscopic systems with our data alone and in combination with catalogue data. From our literature search, we did not fail to detect any systems previously identified as multiple systems. However, there is the possibility that we were not able to identify some multiple systems through our analysis. Our simulations, as seen in Figure 5, are one method to try and account for possible biases in our dataset. However, it is important to note that the raw fractions, F_m as quoted in this paper, should be treated as lower limits, as 64/250 of our targets have only one RV value.

Acknowledgements. We would like to thank the anonymous referee for useful comments that improved this manuscript. Also to Isabelle Baraffe for vital feedback, to Matthew Bate and Gilles Chabrier for helpful and insightful discussions regarding star formation and multiplicity and to Jérôme Bouvier and Estelle Moraux for their input and support of this work and future projects. This publication has made use of VOSA, developed under the Spanish Virtual Observatory project supported from the Spanish MICINN through grant AyA2008-02156. Also the SIMBAD database and VizieR catalogue access tool, CDS, Strasbourg, France.

Appendix A: Temperature scale

The way in which the mass distribution (Figure 2) of our sample was determined was based on effective temperature values in combination with model predictions. When there was no effective temperature value from da Silva et al. (2009), we used the spectral type of that target as an indication for its effective temperature and took the median value for all available targets with the same spectral type in that age bin. If there were no other targets within that spectral type bin a value was constructed through linear interpolation, using the nearest earlier- and later-spectral type. Figure A.1 shows the range of effective temperature and spectral type values.

The spread in effective temperature in each spectral type bin, as shown by the grey shaded areas, is generally small across all three age bins, for example, for the later-types, which is smaller than the spread for younger objects reported in Bayo et al. (2011), which are up to ± 150 K. The largest apparent spread is for the G3 spectral type bin at <20 Myr; it is caused by two values: 4722 K and 5759 K. The result is anomalous, and therefore, any necessary interpolation within the regime G2-G8 was conducted linearly using the two effective temperature values of 5988 K and 5344 K as boundaries, which is in accordance with the trend of the data.

Appendix B: Notes on individual sources

In Appendix B.1 we comment on the individual sources that show RV variation above σ_s , 0.89 km s^{-1} . Appendix B.2 shows the results from an archival search for any existing multiplicity flags. In Appendix B.3 we comment on the data used to identify SB2 and SB3 systems in this work. Appendix B.4 describes further analysis conducted in the cases of potential SB2/SB3 systems to remove false detections from deformities in the CCF profiles.

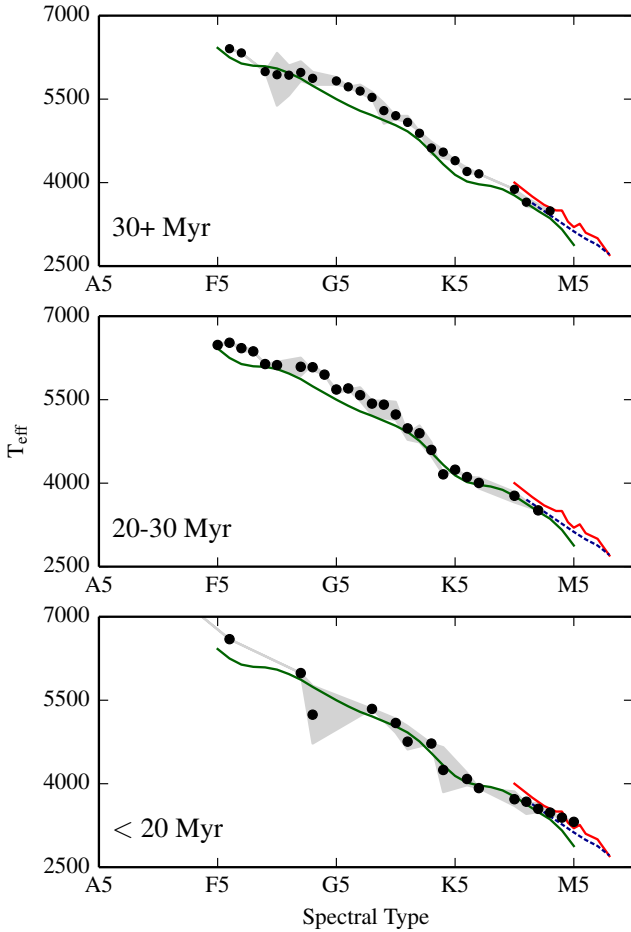


Fig. A.1. Spectral type versus the effective temperature for all stars used in this analysis. The stars have been binned in three different age bins, as indicated in each panel. The grey shaded area represents the range of values within each spectral bin; the black marker is the mean value. Also plotted are the results of Pecaut & Mamajek (2013) – green line, Luhman et al. (2003) – dotted blue line, and Bayo et al. (2011) – solid red line for comparison.

B.1. Archival RV values

Values quoted below, calculated in this work, are average values from all available UVES and FEROS data; their uncertainties are one standard deviation in the following form: $RV \pm \sigma \text{ km s}^{-1}$.

HD 59169: There are only two available epochs for this object: one is from UVES data and the other is FEROS data producing a value of $34.3 \pm 5.4 \text{ km s}^{-1}$. However, this is a significant change in RV, and therefore, it remains a potential multiple system.

AU Mic: There are four data epochs in our own dataset, three from UVES, one from FEROS (-5.1, -5.2, -4.9, and -4.0 km s^{-1}) producing a value of $-4.8 \pm 0.5 \text{ km s}^{-1}$, which is not a significant variation. If one looks at the values from the literature (1.2 ± 1.3 , 15.6 and $-4.5 \pm 1.3 \text{ km s}^{-1}$) there is one value that is significantly different from the others, 15.6 . However, after private communication with John E. Gizis, it is apparent that the 1σ uncertainties are $\approx 17 \text{ km s}^{-1}$, making this value compatible with all others. Therefore, this target is not considered as a multiple system

candidate.

V1005 Ori: This target has a value of $19.0 \pm 0.3 \text{ km s}^{-1}$ from three UVES epochs, which is a variation well below $1\sigma_s$. However, there are seven values from the literatures; which when evaluated together show clear RV variability. Therefore, this target is considered a multiple system candidate.

GSC 09420-00948: There are four UVES data epochs for this target, producing a value of $12.7 \pm 3.2 \text{ km s}^{-1}$. In combination with this, there are two values from Malaroda et al. (2006): 5.0 and 17.1 km s^{-1} . However, these do not have any quoted uncertainties. Because the variation in RV value is larger than σ_s , even without the use of archival data, it remains a potential multiple system.

HD 104467: This target has a value of $13.3 \pm 3.1 \text{ km s}^{-1}$ from both UVES and FEROS data. There are also two values from VizieR: 12.3 ± 1.4 (Torres et al. 2006) and $15.4 \pm 1.0 \text{ km s}^{-1}$ (Kharchenko et al. 2007). The values from the literature are consistent with our derived values but this target remains a potential multiple system due to the high standard deviation.

CD-363202: This target only has one observation one from FEROS data, producing a value of $5.2 \pm 0.9 \text{ km s}^{-1}$ and one value from the catalogue search, $25.6 \pm 1.0 \text{ km s}^{-1}$ (Torres et al. 2006). This is a huge variation in RV; however, it has an extremely high $v\sin i$ value of $170 \pm 17 \text{ km s}^{-1}$ (Torres et al. 2006), which severely limits the accuracy of the RV determination. For this reason it is not considered as a multiple system candidate.

AK Pic: There are two observations for this target producing a value of $35.9 \pm 0.9 \text{ km s}^{-1}$. There are six values from VizieR; four of which have associated uncertainties: 32.3 ± 0.4 , 32.1 ± 0.5 , 32.2 ± 1.5 , and $28.1 \pm 2.1 \text{ km s}^{-1}$. These are more than 3σ , $< 33.1 \text{ km s}^{-1}$, below our derived value, using their upper uncertainty limits. Therefore, this target is a potential multiple system.

BD+012447: This target only has one value calculated in this work, $7.7 \pm 0.9 \text{ km s}^{-1}$. However, there are seven values from VizieR, two of which have associated uncertainties: 8.3 ± 0.2 and $9.1 \pm 0.6 \text{ km s}^{-1}$. These values agree with our derived values, and therefore, this target is not considered as a multiple system candidate.

CD-2711535: There are two observations for this target; it has a calculated RV value of $-6.9 \pm 1.4 \text{ km s}^{-1}$. This standard deviation is well above the average for the sample (0.89 km s^{-1}). There are also two values in VizieR, -6.4 ± 1.0 and $-1.1 \pm 1 \text{ km s}^{-1}$ from Torres et al. (2006) and Song et al. (2012), respectively. The latter value significantly varies from our derived value, and therefore, this target is considered a potential multiple system.

GJ 3305: This target has three observations. It has a calculated RV value of $23.8 \pm 0.5 \text{ km s}^{-1}$. There is one value in VizieR 17.6 km s^{-1} from Reid et al. (1995). However, after private communication with John E. Gizis, it is apparent that the 1σ uncertainties are $\approx 17 \text{ km s}^{-1}$ for this work, and, therefore, this apparent variation is consistent. It is not considered as a member of β -Pic with new RV data from this work. It is a known extremely eccentric multiple system with an eccentricity of 0.06 and a period of 21.5 yr (Delorme et al. 2012).

BD-211074B: This target has three observations; it has a calculated RV value of $21.6 \pm 0.6 \text{ km s}^{-1}$. There are two values from the VizieR 20.0 and 31.7 km s^{-1} from [Reid et al. \(1995\)](#). However, after private communication with John E. Gizis, it is apparent that the 1σ uncertainties are $\approx 17 \text{ km s}^{-1}$ for this work, and therefore, this apparent variation is consistent. Therefore, this target is not considered as a multiple system candidate.

PX Vir: [Griffin \(2010\)](#) determined the spectroscopic orbit of this system (216.48 day). In addition to this, we have one value of $-13.3 \pm 0.89 \text{ km s}^{-1}$, and there are ten values from the VizieR, of which six have associated uncertainties. There are two values from [Maldonado et al. \(2010\)](#) that have a huge variation, which are much higher than the level of uncertainty at -13.1 ± 0.1 and $-2.6 \pm 0.1 \text{ km s}^{-1}$, and agrees with the work of [Griffin \(2010\)](#). Therefore, this target is classified as a multiple system in this work.

GSC 08077-01788: This target has two observations; it has a calculated RV value of $17.6 \pm 0.8 \text{ km s}^{-1}$. There are two values from VizieR, ([Torres et al. 2006](#)): $24.0 \pm 1.0 \text{ km s}^{-1}$ and ([Kordopatis et al. 2013](#)): $-6.9 \pm 4.1 \text{ km s}^{-1}$. This is a very large variation, and therefore, this target is considered a multiple system in this work.

B.2. Archival multiplicity flags

In addition to querying for any existing RV values, we also queried for multiplicity flags from catalogues using VizieR ([Dommangé & Nys \(2002\)](#); [Malkov et al. \(2006\)](#); [Pourbaix et al. \(2004\)](#); [Worley & Douglass \(1996\)](#)), whether the system has previously been identified to have one or more companions. Out of our sub-sample of the overall SACY sample and probing only the SB systems, we found the previous multiplicity results:

HD 33999: This is a previously known triple-lined system ([Dommangé & Nys 2002](#)) which has been flagged in previous SACY work and identified in this work as well.

PX Vir: As discussed in Section B.1, this is a previously identified spectroscopic multiple system which agrees with the variation seen in our catalogue search.

B.3. Definite SB2 and SB3 candidates

Below are any details on the data of positively identified SB2 and SB3 candidates; these targets show a clear double peak in the output of the CCF. The literature was also queried to use any potential existing information.

HD 155177: There are four available data epochs for this object over a wide range of dates (2007-04-19, 2008-10-26, 2012-05-09, and 2012-06-14). There are two clear peaks that vary across the data epochs indicating strong it is a binary system. No obvious note of spectroscopic multiplicity in the literature.

HD 33999: As mentioned in Appendix B.2, this is a previously known triple-lined multiple system.

HD 309751: There is only one epoch of data available for this object (2011-11-20); however, the produced CCF profile is

extremely clear to identify it as an SB2 system. [Torres et al. \(2006\)](#) identified this as an SB2 system.

BD-20951: There are two epochs of data for this target (2012-07-17, 2012-07-31). There are two clear peaks in the CCFs, indicating strongly it is a bound binary system. To the best of our knowledge, there is no note of spectroscopic multiplicity in the literature.

V4046-Sgr: There are a great many data epochs for this object and it is a well known and studied spectroscopic binary system (e.g., [Quast et al. \(2000\)](#); [Argiroffi et al. \(2012\)](#); [Donati et al. \(2011\)](#)).

HD 217379: There is only one epoch of data for this object (2010-05-25). Despite this, the CCF provides a clear result that this is a triple-lined system; the signal-to-noise is ~ 200 , and all three peaks are well above the noise level. [Torres et al. \(2006\)](#) identified this as a triple-lined (SB3) spectroscopic system.

TWA 14: There are two data epochs available for this object (2012-05-22, 2012-06-04). The output of the CCF shows two peaks; however the profiles are merged. The two peaks have different depths in each data epoch and appear to switch position between the two epochs, indicating it is a bound binary system. [Weinberger et al. \(2013\)](#) and identified [Jayawardhana et al. \(2006\)](#) this as a double-lined (SB2) system.

TWA 20: There are three epochs of data for this target (2012-05-07, 2012-05-22, and 2012-07-03). There are two strong peaks in all of the CCFs from the RED arm of UVES; the blue is very noisy due to the spectral type of the star, M3. In addition, [Jayawardhana et al. \(2006\)](#) identify this is a SB2 system, and therefore, it is classified as an SB2 system in this work; however it is not considered a member of TW-Hydrae with new RV values.

1RXS J195602.8-320720: There is one epoch of data for this target (2011-10-09). The spectral type of the star is M4, and therefore, the CCF output is quite noisy; however, there is a clear second peak above the level of the noise in both the results from the RED arm of UVES. To the best of our knowledge, there is no note of spectroscopic multiplicity in the literature.

B.4. Questionable SB2 and SB3 candidates

Initially, some targets were flagged as potential multiple systems, as shown in Table B.1. The targets CD-423328, CD-542644 and CP-551885 have previously been identified as having variable rotational behaviour due to the presence of spots ([Kiraga 2012](#)). However, this does not exclude the possibility that they are multiple systems; therefore, we conduct the same analysis for these targets as for those without any variability flag.

For the targets shown in Table B.1, we conducted the following analysis to determine whether the deformity could be the solely the result of spots on the surface of the star.

The intensity of Ca II H (3968.5 Å) and Ca II K (3933.7 Å) emission respond to the amount of non-thermal heating of the chromosphere, which can be caused by areas of concentrated magnetic field ([Leighton 1959](#)); therefore, there is a strong link between spot coverage and activity. We can use this to our ad-

Table B.1. Details of all initially flagged potential multiple systems.

Target	SpT	MJD	RV _{blue} (km s ⁻¹)	Relative phase (ϕ) ^a	Period (day) ^b	Variability Type ^c	v sin (i)	Association
CD-423328	K1	56175.398	15.1	-	-	rot	41.0 ^c	CAR
		56179.380	15.3					
CD-433604	K4	54876.233	20.4	0	0.89	-	40.0 ^b	ARG
		56175.381	24.1	0.717				
		56179.371	11.0	0.200				
CD-542644	G5	54898.165	20.8	0	1.5	rot	39.5 ^b	CAR
		55885.322	21.5	0.105				
CP-551885*	G5	54898.158	27.6	0	0.916	rot	44.0 ^b	CAR
		55885.307	24.0	0.674				
GSC 09239-01572	K7	55340.108	16.4	0	1.536	-	41.0 ^b	ECH
		55947.346	12.0	0.337				
		55978.336	8.6	0.513				
		55979.299	13.6	0.140				
HD 30051*	F2	56138.352	-1.5	-	-	-	-	THA
		56139.358	-2.1					
		56140.361	-2.5					
TYC 7605-1429-1	K4	55461.359	30.7	-	0.3514	-	-	ABD
TYC 7627-2190-1	K2	54896.092	25.6	0	0.726	-	-	ABD
		55416.402	27.2	0.680				
TYC 8594-58-1	G8	54880.184	10.8	0	0.982	-	34.1 ^b	ARG
		56082.022	8.2	0.868				
		56107.997	10.9	0.319				

Notes. (*) No longer classified as a member of association with new RV values.^(a) Relative phase values (relative to our first observation) were computed using the MJD values from each observation and period values. ^(b) Messina et al. (2010, 2011). ^(c) Kiraga (2012): Variability Type: rot=rotational variability due to the presence of spots.

vantage in our CCF output to differentiate between spots and merged-SB2 components.

We fitted one Gaussian profile to the CCF output, assuming it was a single star, producing a system velocity (v_{sys}) and then looked for the specific velocities of the deformities in the profile (v_{d1}, v_{d2} , etc.). We then compared the system velocity and deformity velocity values to the line profiles of Ca II H and K; the chromosphere can emit isotropically at the system velocity and have components of emission from the strong areas of magnetism, corresponding to the deformity velocities. If the Ca II H and K lines had a multiple-component structure with peaks corresponding to the values of v_{sys} and v_{d1}, v_{d2} etc. then it is very likely that the candidate multiple system is a single system with strong activity. If this was not the case but the profiles of Ca II H and K had a multiple component structure, we also checked whether the multiple components had peak values corresponding to a multiple-line fit to the CCF, which assume the system is multiple.

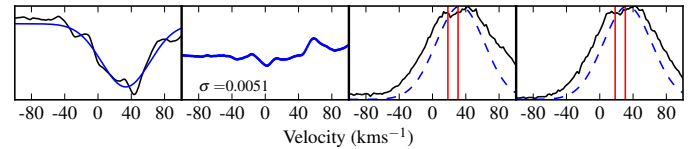
The graphs presented in this section are in the following format. There are four panels for each UVES observation from left to right (1-4).

- **Panel 1:** The CCF output for the BLUE chip of UVES (blue line) and single Gaussian fit (black line). Phase values, ϕ , are shown from Table B.1 where available.
- **Panel 2:** The residuals from each of the fits, all graphs have the same y-axis range for easy comparison of the goodness of fit. The parameter σ represents the average standard deviation in the residuals from the fit.

- **Panel 3:** The normalised flux of chromospheric line Ca II H, 3968.5 Å, in velocity space (black line); overplotted is the normalised and reversed CCF profile from Panel 1 (blue dotted line) as well as v_{sys} and $v_{d1,2}$ (red vertical lines).

- **Panel 4** has the same format as Panel 3 but is at 3933.7 Å, for the chromospheric line Ca II K.

TYC 7605-1429-1: This target was initially identified as a binary candidate due to its abnormal CCF profile. However, TYC 7605-1429-1 only has one epoch of data, which is not conclusive from this analysis, as shown in Figure B.1. It has an extremely broad component with a FWHM of ≈ 62 km s⁻¹, making the RV determination difficult. Torres et al. (2006) quote a value of 28.6 km s⁻¹ which agrees with our derived value of 31.2 ± 4.0 km s⁻¹. Messina et al. (2010) flagged this target as a single system.

**Fig. B.1.** TYC 7605-1429-1: 2012-09-22.

HD 30051: There are three available epochs for this target, 2012-07-30, 2012-07-31, and 2012-08-01. This is an F2-type

star, and therefore, does not have strong chromospheric activity, as shown in the lack of emission in Panels 3 and 4 of Figure B.2. This star was initially classified as a multiple system due to the two component structure of the CCF profile, which potentially consists of a rapid rotator, producing the broad component with a slower-rotating companion, narrow component. However, there is no significant variation in system velocity (-1.5, -2.1 and, -2.5) between observations, making it extremely unlikely to be a close binary system with period > 1 day.

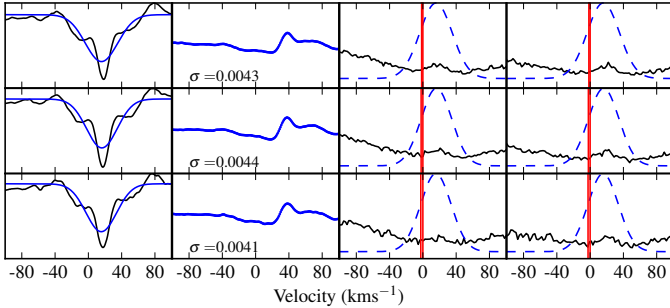


Fig. B.2. HD 30051: 2012-07-30, 2012-07-31, and 2012-08-01.

CD-542644: There are two epochs for this target 2009-03-08 and 2011-11-20, as seen in Figure B.3. The velocities for v_{sys} and $v_{\text{d}1}$ do not correspond well to the shape of the line profiles. The CCF profiles are also quite complex, making it hard to determine the correct velocities. Based on this analysis, we do not consider this target a multiple system.

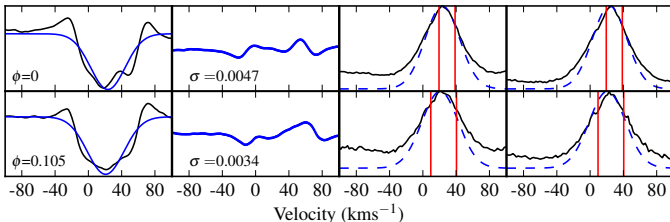


Fig. B.3. CD-542644: 2009-03-08, and 2011-11-20.

CP-551885: There are two epochs for this target 2009-03-08 and 2011-11-20, as seen in Figure B.4. The line profiles displayed in panels 3 and 4 show a clear two component structure. However, the picture we have is confusing; the v_{sys} value agrees well in both epochs; however, $v_{\text{d}1}$ does not. Instead, it is one of the velocities fitted using two Gaussians that matches with the secondary peak $\approx 5 \text{ km s}^{-1}$. In addition to this, if we look at the v_{sys} values, there is no considerable variation: 27.6 ($\phi = 0$), 21.5 ($\phi = 0.674$) and (Torres et al. 2006) 23.1 km s^{-1} from previous work, assuming the period of rotation is synchronised with the orbital period. Based on these arguments, we do not consider this target a multiple system.

CD-423328: There are two epochs for this target 2012-09-05 and 2012-09-09, as seen in Figure B.5. The lines from a two-component Gaussian fit agree with the peaks seen in the profiles of Ca II H and K. Torres et al. (2006) also quote a value of $24.6 \pm 1.0 \text{ km s}^{-1}$, which is hugely different from our value derived from a single Gaussian fit ($15.2 \pm 0.1 \text{ km s}^{-1}$). Kiraga

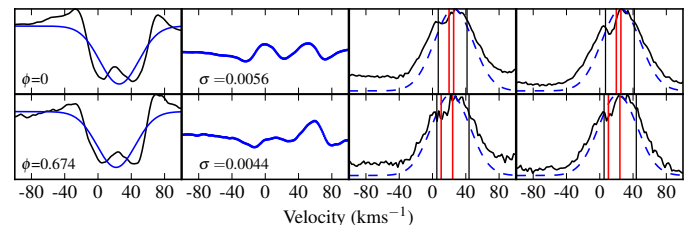


Fig. B.4. CP-551885: 2009-03-08, and 2011-11-20.

(2012) classified this object as rotationally variable due to the presence of spots; however, this does not exclude the possibility that it is a binary system. Due to this line-profile analysis and the variation in RV value, this target is classified as a potential multiple system.

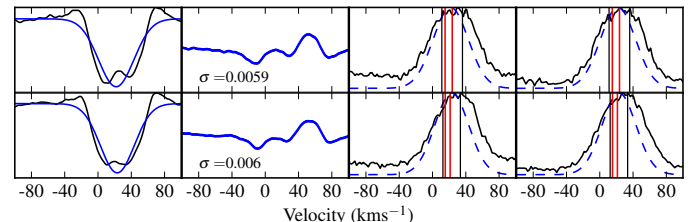


Fig. B.5. CD-423328: 2012-09-05, and 2012-09-09.

CD-433604: There are three available epochs for this target, 2009-02-14, 2012-09-05, and 2012-09-09, as seen in Figure B.6. It is extremely unlikely that it is an SB2 system, as the flux ratio of the two components is variable epoch to epoch (0.97, 0.64, 0.56 respectively). The line profile analysis is inconclusive; epochs 2012-09-05 and 2012-09-09 show a two-component structure in Ca II H and K; however, the derived v_{sys} and $v_{\text{d}1}$ values do not correspond to the peaks of these components. The calculated RV values (20.4, 24.1, and 11.0) are extremely variable, but the fits are poor, as seen in panel 2 of Figure B.6. There is one other existing value (priv. communication, C. A. O. Torres) of 21.4, and therefore, if one considers three of the four values to compute an average, there is no significant variation ($22.0 \pm 1.9 \text{ km s}^{-1}$). At this time, the evidence for multiplicity is not strong enough for us to consider this target as a multiple system.

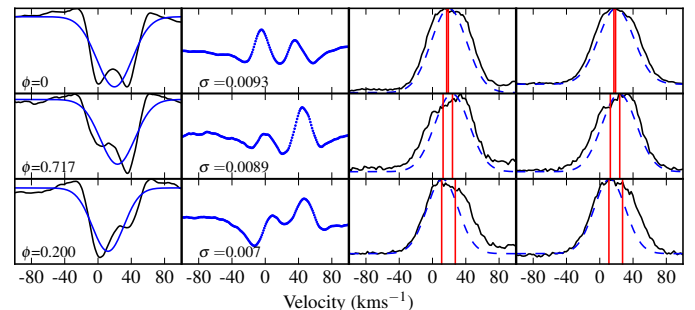


Fig. B.6. CD-433604: 2009-02-14, 2012-09-05, and 2012-09-09.

GSC 09239-01572: There are four epochs available for this object, 2010-05-24, 2012-01-21, 2012-02-21, and 2012-02-22. In Figure B.7, one can see the agreement between the deformity velocities and the line profiles of Ca II H and K is extremely good for all four epochs. On this basis, we conclude that the CCF profile is the result of star spots as opposed to multiplicity.

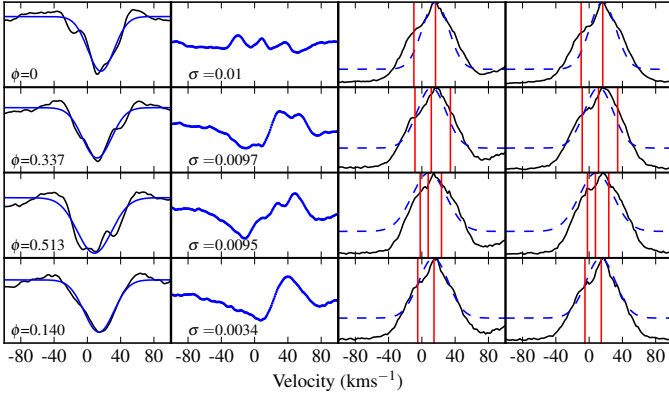


Fig. B.7. GSC 09239-01572: 2010-05-24, 2012-01-21, 2012-02-21, and 2012-02-22.

TYC 7627-2190-1: There are two epochs available for this object: 2009-03-06 and 2010-08-08, as seen Figure B.8. From the fitting of a single system velocity to the profiles there is no significant variation between the observations (25.6 and 27.2). The value of the system velocity is extremely close to that of the deformity velocity; this makes it extremely difficult to see the separate components in this analysis. However, we only have two epochs, and therefore based on this evidence, we do not classify this as a multiple system.

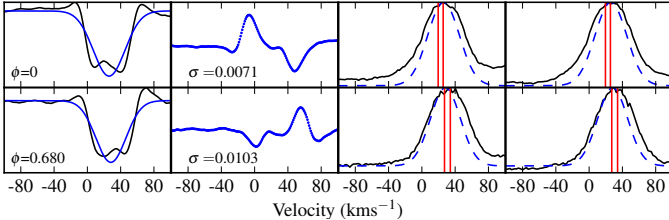


Fig. B.8. TYC 7627-2190-1: 2009-03-06, and 2010-08-08.

TYC 8594-58-1: There are three epochs of data for this target: 2009-02-18, 2012-06-04 and 2012-06-29. However, much like TYC7627-2190, the value of the deformity velocity is extremely close to the system velocity, and therefore, seeing the two components separately is extremely difficult. There is no significant variation in the system velocity between all three epochs (10.8, 8.2, and 10.9, respectively). Figure B.9 also shows the velocities when fitting the CCF with two Gaussians, as shown as black vertical lines. Neither of these techniques provide strong evidence for or against the multiplicity of the system. Therefore, as it statistically much more likely to be a single system, it is not considered a multiple system in this work.

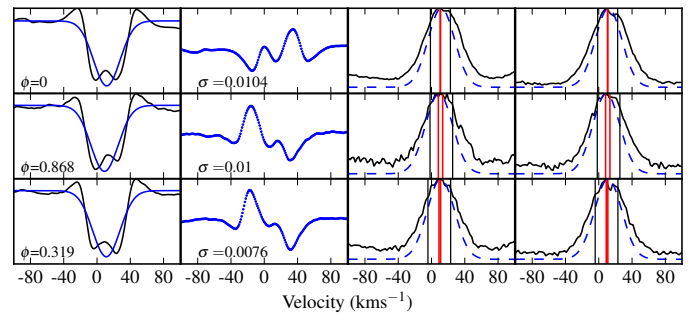


Fig. B.9. TYC 8594-58-1: 2009-02-18, 2012-06-04, and 2012-06-29.

References

- Andersen, J., Nordstrom, B., Ardeberg, A., et al. 1985, A&AS, 59, 15
 Anderson, E. & Francis, C. 2012, Astronomy Letters, 38, 331
 Argiroffi, C., Maggio, A., Montmerle, T., et al. 2012, ApJ, 752, 100
 Baines, D., Oudmaijer, R. D., Porter, J. M., & Pozzo, M. 2006, MNRAS, 367, 737
 Baraffe, I., Chabrier, G., Allard, F., & Hauschildt, P. 2003, in IAU Symposium, Vol. 211, Brown Dwarfs, ed. E. Martín, 41
 Baraffe, I., Chabrier, G., Allard, F., & Hauschildt, P. H. 1998, A&A, 337, 403
 Baranne, A., Queloz, D., Mayor, M., et al. 1996, A&AS, 119, 373
 Barrado Y Navascués, D. 2006, A&A, 459, 511
 Barrado y Navascués, D., Stauffer, J. R., Song, I., & Caillault, J.-P. 1999, ApJ, 520, L123
 Bate, M. R., Bonnell, I. A., & Bromm, V. 2002, MNRAS, 336, 705
 Bayes, M. & Price, M. 1763, Royal Society of London Philosophical Transactions Series I, 53, 370
 Bayo, A., Barrado, D., Stauffer, J., et al. 2011, A&A, 536, A63
 Bayo, A., Rodrigo, C., Barrado Y Navascués, D., et al. 2008, A&A, 492, 277
 Bobylev, V. V., Goncharov, G. A., & Bajkova, A. T. 2006, Astronomy Reports, 50, 733
 Burgasser, A. J., Kirkpatrick, J. D., Reid, I. N., et al. 2003, ApJ, 586, 512
 Casagrande, L., Schönrich, R., Asplund, M., et al. 2011, A&A, 530, A138
 Chini, R., Hoffmeister, V. H., Nasseri, A., Stahl, O., & Zinnecker, H. 2012, MNRAS, 424, 1925
 da Silva, L., Torres, C. A. O., de La Reza, R., et al. 2009, A&A, 508, 833
 de Bruijne, J. H. J. & Eilers, A.-C. 2012, A&A, 546, A61
 Delorme, P., Lagrange, A. M., Chauvin, G., et al. 2012, A&A, 539, A72
 Dommangé, J. & Nys, O. 2002, VizieR Online Data Catalog, 1274, 0
 Donati, J.-F., Gregory, S. G., Montmerle, T., et al. 2011, MNRAS, 417, 1747
 Duquennoy, A. & Mayor, M. 1991, A&A, 248, 485
 Eggleton, P. P. & Kisselava-Eggleton, L. 2006, Ap&SS, 304, 75
 Fischer, D. A. & Marcy, G. W. 1992, ApJ, 396, 178
 Ghez, A. M., McCarthy, D. W., Patience, J. L., & Beck, T. L. 1997, ApJ, 481, 378
 Ghez, A. M., Neugebauer, G., & Matthews, K. 1993, AJ, 106, 2005
 Gontcharov, G. A. 2006, Astronomical and Astrophysical Transactions, 25, 145
 Gray, D. F. 1976, The observation and analysis of stellar photospheres
 Griffin, R. F. 2010, The Observatory, 130, 125
 Halbwachs, J.-L. 2001, Ecole de Goutelas, 23, 1
 Henry, T. J. & McCarthy, Jr., D. W. 1990, ApJ, 350, 334
 Hubber, D. A. & Whitworth, A. P. 2005, A&A, 437, 113
 Ivanov, G. A. 2008, Kinematika i Fizika Nebesnykh Tel, 24, 480
 Jayawardhana, R., Coffey, J., Scholz, A., Brandeker, A., & van Kerwijk, M. H. 2006, ApJ, 648, 1206
 Jenkins, J. S., Murgas, F., Rojo, P., et al. 2011, A&A, 531, A8
 Jumper, P. H. & Fisher, R. T. 2013, ApJ, 769, 9
 Kharchenko, N. V., Scholz, R.-D., Piskunov, A. E., Röser, S., & Schilbach, E. 2007, Astronomische Nachrichten, 328, 889
 King, R. R., Goodwin, S. P., Parker, R. J., & Patience, J. 2012a, MNRAS, 427, 2636
 King, R. R., Parker, R. J., Patience, J., & Goodwin, S. P. 2012b, MNRAS, 421, 2025
 Kiraga, M. 2012, VizieR Online Data Catalog, 1206, 20067
 Kordopatis, G., Gilmore, G., Steinmetz, M., et al. 2013, AJ, 146, 134
 Kouwenhoven, M. B. N., Brown, A. G. A., & Kaper, L. 2007, VizieR Online Data Catalog, 346, 40581
 Koyama, K., Hamaguchi, K., Ueno, S., Kobayashi, N., & Feigelson, E. D. 1996, PASJ, 48, L87

- Kroupa, P. 1995, MNRAS, 277, 1522
- Lagrange, A.-M., Meunier, N., Chauvin, G., et al. 2013, A&A, 559, A83
- Larson, R. B. 1969, MNRAS, 145, 271
- Leighton, R. B. 1959, ApJ, 130, 366
- Lopez Martí, B., Jimenez Esteban, F., Bayo, A., et al. 2013, A&A, 551, A46
- Luhman, K. L. 2004, ApJ, 602, 816
- Luhman, K. L., Stauffer, J. R., Muench, A. A., et al. 2003, ApJ, 593, 1093
- Malaroda, S., Levato, H., & Galliani, S. 2006, VizieR Online Data Catalog, 3249, 0
- Maldonado, J., Martínez-Arnáiz, R. M., Eiroa, C., Montes, D., & Montesinos, B. 2010, A&A, 521, A12
- Malkov, O. Y., Oblak, E., Snegireva, E. A., & Torra, J. 2006, A&A, 446, 785
- Marks, M., Leigh, N., Giersz, M., et al. 2014, MNRAS, 441, 3503
- Mason, B. D., Henry, T. J., Hartkopf, W. I., ten Brummelaar, T., & Soderblom, D. R. 1998, AJ, 116, 2975
- Mayor, M. & Mermilliod, J. C. 1984, in IAU Symposium, Vol. 105, Observational Tests of the Stellar Evolution Theory, ed. A. Maeder & A. Renzini, 411
- Melo, C. H. F. 2003, A&A, 410, 269
- Messina, S., Desidera, S., Lanzaflame, A. C., Turatto, M., & Guinan, E. F. 2011, A&A, 532, A10
- Messina, S., Desidera, S., Turatto, M., Lanzaflame, A. C., & Guinan, E. F. 2010, A&A, 520, A15
- Neuhäuser, R., Briceño, C., Comerón, F., et al. 1999, A&A, 343, 883
- Nguyen, D. C., Brandeker, A., van Kerkwijk, M. H., & Jayawardhana, R. 2012, The Astrophysical Journal, 745, 119
- Parker, R. J., Goodwin, S. P., Kroupa, P., & Kouwenhoven, M. B. N. 2009, MNRAS, 397, 1577
- Pecaut, M. J. & Mamajek, E. E. 2013, ApJS, 208, 9
- Pourbaix, D., Tokovinin, A. A., Batten, A. H., et al. 2004, A&A, 424, 727
- Quast, G. R., Torres, C. A. O., de La Reza, R., da Silva, L., & Mayor, M. 2000, in IAU Symposium, Vol. 200, IAU Symposium, 28P
- Queloz, D. 1995, in IAU Symposium, Vol. 167, New Developments in Array Technology and Applications, ed. A. G. D. Philip, K. Janes, & A. R. Upgren, 221
- Raghavan, D., McAlister, H. A., Henry, T. J., et al. 2010, ApJS, 190, 1
- Reid, I. N., Hawley, S. L., & Gizis, J. E. 1995, AJ, 110, 1838
- Rocha-Pinto, H. J., Flynn, C., Scalo, J., et al. 2004, A&A, 423, 517
- Sana, H., de Koter, A., de Mink, S. E., et al. 2013, A&A, 550, A107
- Sana, H. & Evans, C. J. 2011, in IAU Symposium, Vol. 272, IAU Symposium, ed. C. Neiner, G. Wade, G. Meynet, & G. Peters, 474–485
- Sestito, P., Palla, F., & Randich, S. 2008, A&A, 487, 965
- Siebert, A., Williams, M. E. K., Siviero, A., et al. 2011, AJ, 141, 187
- Siess, L., Dufour, E., & Forestini, M. 2000, A&A, 358, 593
- Sollima, A., Beccari, G., Ferraro, F. R., Fusi Pecci, F., & Sarajedini, A. 2007, MNRAS, 380, 781
- Song, I., Zuckerman, B., & Bessell, M. S. 2012, AJ, 144, 8
- Strassmeier, K., Washuettl, A., Granzer, T., Scheck, M., & Weber, M. 2000, A&AS, 142, 275
- Tokovinin, A., Thomas, S., Sterzik, M., & Udry, S. 2006, A&A, 450, 681
- Torres, C. A. O., Quast, G. R., da Silva, L., et al. 2006, A&A, 460, 695
- Torres, C. A. O., Quast, G. R., Melo, C. H. F., & Sterzik, M. F. 2008, Young Nearby Loose Associations, ed. B. Reipurth, 757
- Turon, C., Creze, M., Egret, D., et al. 1993, Bulletin d'Information du Centre de Données Stellaires, 43, 5
- Viana Almeida, P., Santos, N. C., Melo, C., et al. 2009, A&A, 501, 965
- Walter, F. M., Brown, A., Mathieu, R. D., Myers, P. C., & Vrba, F. J. 1988, AJ, 96, 297
- Weinberger, A. J., Anglada-Escudé, G., & Boss, A. P. 2013, ApJ, 762, 118
- White, R. J., Gabor, J. M., & Hillenbrand, L. A. 2007, AJ, 133, 2524
- Worley, C. E. & Douglass, G. G. 1996, VizieR Online Data Catalog, 1237, 0
- Zinnecker, H. & Preibisch, T. 1994, A&A, 292, 152
- Zuckerman, B., Song, I., Bessell, M. S., & Webb, R. A. 2001, ApJ, 562, L87

Appendix C: Radial velocity values

Table C.1. Summary table of all radial velocity values used in this work for single and SB1 systems.

ID	RA	DEC	N. of Obs.	RV (km s ⁻¹)	$\sigma^{1,2}$	Reference ³
AB Doradus members						
HD 6569	01:06:26.2	-14:17:47	2	7.55	0.02	
BD-12243	01:20:32.3	-11:28:04	2	10.26	0.35	
CD-46644	02:10:55.4	-46:03:59	1	25.78	0.89	
				25.7	-	t
HD 16760B	02:42:21.0	+38:37:21	1	-3.46	0.89	
HD 16760	02:42:21.3	+38:37:07	1	-3.19	0.89	
HD 17332B	02:47:27.2	+19:22:21	2	4.41	0.65	
HD 17332A	02:47:27.4	+19:22:19	1	3.91	0.89	
				4.5	1.3	a
				4.4	0.2	f
				4.3	0.1	f
				3.76	0.8	g
IS Eri	03:09:42.3	-09:34:47	2	14.46	0.14	
HD 24681	03:55:20.4	-01:43:45	1	18.02	0.89	
HD 25457	04:02:36.7	-00:16:08	2	17.62	0.36	
HD 31652	04:57:22.3	-09:08:00	1	22.61	0.89	
CD-401701	05:02:30.4	-39:59:13	3	28.4	0.25	
				27.8	1.0	j
HD 32981	05:06:27.7	-15:49:30	1	25.64	0.89	
HD 293857	05:11:09.7	-04:10:54	1	20.28	0.89	
HD 35650	05:24:30.2	-38:58:11	4	32.32	0.53	
				31.3	0.3	f
UX Col	05:28:56.5	-33:28:16	2	30.07	0.38	
				30.1	0.1	j
CD-342331	05:35:04.1	-34:17:52	3	30.48	0.14	
				30.4	1.0	j
CD-481893	05:36:55.1	-47:57:48	3	30.98	1.21	
				32.2	0.2	g
				32.2	B	n
UY Pic	05:36:56.9	-47:57:53	3	32.31	0.22	
WX Col	05:37:12.9	-42:42:56	4	31.38	0.18	
TYC 7604-1675-1	05:37:13.2	-42:42:57	2	30.47	0.14	
TYC 4779-394-1	05:38:56.6	-06:24:41	1	22.88	0.89	
CP-19878	05:39:23.2	-19:33:29	2	27.8	0.91	
TYC 7605-1429-1	05:41:14.3	-41:17:59	1	30.7	0.89	
TZ Col	05:52:16.0	-28:39:25	2	28.71	0.25	
				31.1	1.0	j
BD-131328	06:02:21.9	-13:55:33	1	25.43	0.89	
CD-342676	06:08:33.9	-34:02:55	3	30.47	0.69	
				31.1	1.0	j
CD-352722	06:09:19.2	-35:49:31	3	32.03	0.08	
				31.4	0.4	j
HD 45270	06:22:30.9	-60:13:07	4	31.63	0.32	
AK Pic	06:38:00.4	-61:32:00	2	35.87	0.91	
				32.3	0.35	c
				28.1	-	e
				32.1	0.5	f
				32.2	1.5	g
				28.1	2.1	g
				35.0	1.0	j
CD-611439	06:39:50.0	-61:28:42	1	31.38	0.89	

ID	RA	DEC	N. of Obs.	RV (km s ⁻¹)	$\sigma^{1,2}$	Reference ³
TYC 7627-2190-1	06:41:18.5	-38:20:36	2	31.7	1.0	j
GSC 08544-01037*	06:47:53.4	-57:13:32	3	28.0	0.8	
CD-571654	07:10:50.6	-57:36:46	3	30.0	0.43	
				29.22	0.14	
				29.7	1.0	j
V429 Gem	07:23:43.6	+20:24:59	2	7.39	0.43	
				9.3	-	b
HD 59169	07:26:17.7	-49:40:51	2	34.29	5.38	
CD-8480	07:30:59.5	-84:19:28	1	23.23	0.89	
				24.2	0.8	j
HD 64982	07:45:35.6	-79:40:08	2	25.66	0.01	
BD+012447	10:28:55.5	+00:50:28	1	7.71	0.89	
				18.3	-	b
				12.7	-	b
				11.8	-	b
				8.4	-	b
				9.9	-	d
				8.3	0.2	f
				9.1	0.6	g
PX Vir	13:03:49.7	-05:09:43	1	-13.3	0.89	
				-10.8	0.3	f
				0.0	-	g
				-13.1	0.08	k
				-2.6	0.09	k
				-13.1	1.7	m
				-9.21	A	n
				-8.2	-	p
				-5.8	-	p
				7.9	-	q
				0.0	5.0	s
HD 139751	15:40:28.4	-18:41:46	1	-7.6	0.89	
HIP 81084	16:33:41.6	-09:33:12	1	-14.66	0.89	
HD 152555	16:54:08.1	-04:20:25	2	-16.44	0.01	
HD 178085	19:10:57.9	-60:16:20	1	8.45	0.89	
				8.1	1.1	j
TYC 486-4943-1	19:33:03.8	+03:45:40	1	-20.69	0.89	
BD-034778	20:04:49.4	-02:39:20	2	-16.46	0.01	
HD 199058	20:54:21.1	+09:02:24	2	-19.54	0.17	
TYC 1090-543-1	20:54:28.0	+09:06:07	2	-19.18	0.13	
HD 201919	21:13:05.2	-17:29:13	3	-7.39	0.24	
				-7.4	1.0	j
HD 218860	23:11:52.0	-45:08:11	2	9.92	0.32	
				11.2	1.3	j
HD 222575	23:41:54.2	-35:58:39	1	10.83	0.89	
				11.1	1.7	j
HD 224228	23:56:10.5	-39:03:07	4	13.48	0.59	

Argus members

CD-292360	05:34:59.2	-29:54:04	3	25.71	0.31	
				26.0	1.0	j
CD-283434	06:49:45.4	-28:59:17	1	26.68	0.89	
				26.7	1.0	j
CD-422906	07:01:53.4	-42:27:56	4	23.73	0.23	
				23.7	1.0	j
CD-482972	07:28:22.0	-49:08:38	1	18.85	0.89	
				21.1	1.0	j

ID	RA	DEC	N. of Obs.	RV (km s ⁻¹)	$\sigma^{1,2}$	Reference ³
HD 61005	07:35:47.5	-32:12:14	2	22.36	0.21	
CD-483199	07:47:26.0	-49:02:51	5	17.68	0.31	
				18.5	1.0	j
CD-433604	07 48 49.8	-43 27 06	3	22.0	1.91	
TYC 8561-970-1	07:53:55.5	-57:10:07	4	15.85	0.18	
RXS J082952.7-514030	08:29:51.9	-51:40:40	1	16.15	0.89	
PMM 6974	08:34:18.1	-52:15:58	1	15.1	0.89	
TYC 8568-407-1	08:34:20.5	-52:50:05	1	16.88	0.89	
1RXS J083502.7-521339	08:35:01.2	-52:14:01	1	15.4	0.89	
ASAS J083655-5308.5	08:36:55.0	-53:08:34	1	14.67	0.89	
TYC 8568-2261-1	08:37:51.6	-53:45:46	1	14.58	0.89	
CD-52 2467	08:38:22.9	-52:56:48	1	15.14	0.89	
PMM 686	08:39:22.6	-53:55:06	1	15.18	0.89	
V364 Vel	08:39:53.0	-52:57:57	1	15.26	0.89	
PMM 8415	08:40:16.3	-52:56:29	1	14.79	0.89	
VXR PSPC 22a	08:40:49.1	-53:37:45	1	14.14	0.89	
TYC 8569-3687-1	08:43:00.4	-53:54:08	1	16.13	0.89	
V376 Vel	08:44:05.2	-52:53:17	1	13.61	0.89	
			1	14.74	0.89	
CD-572315	08:50:08.1	-57:45:59	5	11.93	0.86	
				11.7	0.7	j
TYC 8594-58-1	09:02:03.9	-58:08:50	3	10.0	1.53	
BD-202977	09:39:51.4	-21:34:17	1	17.87	0.89	
TYC 9217-641-1	09:42:47.4	-72:39:50	2	6.17	0.72	
				6.7	1.0	j
CD-395833	09:47:19.9	-40:03:10	3	14.87	0.33	
HD 309851	09:55:58.3	-67:21:22	4	7.39	0.4	
				6.6	1.0	j
CD-74673	12:20:34.4	-75:39:29	1	4.68	0.89	
				0.6	0.8	j
CD-75652	13:49:12.9	-75:49:48	5	-1.03	0.26	
				-0.9	1.0	j
HD 129496	14:46:21.4	-67:46:16	1	-11.0	0.89	
NY Aps	15:12:23.4	-75:15:16	4	-3.07	0.26	
				-3.5	0.1	j
CD-529381	20:07:23.8	-51:47:27	1	-13.66	0.89	
				-13.3	1.0	j

 β -Pic members

HIP 10679	02:17:24.7	+28:44:30	1	5.32	0.89	
				3.9	1.3	a
				5.0	1.3	g
				5.0	0.2	s
GSC 08056-00482	02:36:51.5	-52:03:04	1	13.84	0.89	
				16.0	0.1	j
BD+05378*	02:41:25.9	+05:59:18	1	7.31	0.89	
				10.0	-	n
GJ 3305*	04:37:37.5	-02:29:28	3	23.84	0.47	
				17.6	-	d
V1005 Ori	04:59:34.8	+01:47:01	3	18.95	0.33	
				39.0	-	b
				32.4	-	b
				18.2	-	b
				37.2	-	d
				18.7	3.3	f
				22.0	5.1	g

ID	RA	DEC	N. of Obs.	RV (km s ⁻¹)	$\sigma^{1,2}$	Reference ³
CD-571054	05:00:47.1	-57:15:25	2	30.5	5.1	s
				19.48	0.47	
BD-211074B	05:06:49.5	-21:35:04	3	19.4	0.3	j
				21.55	0.55	
BD-211074A	05:06:49.9	-21:35:09	2	20.0	-	d
				31.7	-	d
TYC 112-917-1	05:20:00.3	+06:13:04	3	21.22	0.31	
TYC 112-1486-1	05:20:31.8	+06:16:11	3	18.76	0.13	
V1311 Ori*	05:32:04.5	-03:05:29	3	18.52	0.23	
				18.0	-	t
AO Men	06:18:28.2	-72:02:41	5	23.84	0.55	
				16.18	0.19	
TWA 22	10:17:26.9	-53:54:27	2	16.2	1.0	u
				13.49	0.1	
HD 139084B	15:38:56.8	-57:42:19	1	3.03	0.89	
				0.1	2.0	j
V343 Nor	15:38:57.5	-57:42:27	3	3.32	2.23	
				3.1	0.8	f
CD-2711535	17:15:03.6	-27:49:40	2	3.6	0.95	g
				4.2	1.4	j
CD-547336	17:29:55.1	-54:15:49	4	2.4	-	l
				-6.9	1.36	
HD 164249	18:03:03.4	-51:38:56	1	-6.4	1.0	j
				-1.1	1.8	r
GSC 07396-00759	18:14:22.1	-32:46:10	1	0.95	0.67	
				1.6	1.4	j
TYC 9073-762-1	18:46:52.6	-62:10:36	3	-0.5	3.7	r
				-0.67	0.89	
CD-2613904	19:11:44.7	-26:04:09	1	-6.05	0.89	
				2.56	0.78	
HD 181327	19:22:58.9	-54:32:17	3	-9.72	0.89	
				-0.72	0.29	
TYC 7443-1102-1	19:56:04.4	-32:07:38	2	-6.32	0.04	
				-4.64	0.24	
1RXS J200136.9-331307	20:01:37.2	-33:13:14	3	-4.82	0.49	
				1.2	1.3	a
AU Mic	20:45:09.3	-31:20:24	4	15.6	-	d
				-4.5	1.3	g
AZ Cap	20:56:02.7	-17:10:54	3	-7.74	0.88	
				-6.9	1.0	j
CP-722713	22:42:48.9	-71:42:21	1	7.78	0.89	
				8.6	0.5	j
WW PsA	22:44:57.8	-33:15:01	3	1.95	0.83	
				2.2	1.0	j
TX PsA	22:45:00.0	-33:15:26	2	2.97	0.32	
				1.13	0.99	
BD-136424	23:32:30.9	-12:15:52	3	1.8	0.7	j
				-	-	

Carina members

HD 269620	05:29:27.1	-68:52:05	5	19.27	0.41	
				18.7	1.0	j
HD 42270	05:53:29.3	-81:56:53	3	16.57	0.33	
				16.7	0.6	j
CD-482324	06:28:06.1	-48:26:53	1	24.57	0.89	
				24.9	1.0	j
HD 49855*	06:43:46.2	-71:58:35	4	20.83	0.14	

ID	RA	DEC	N. of Obs.	RV (km s ⁻¹)	$\sigma^{1,2}$	Reference ³
CD-571709	07:21:23.7	-57:20:37	4	20.1 19.9 20.7 23.32	0.5 0.5 0.1 0.31	f g j
CD-423328 ^a	07:33:21.2	-42:55:42	2	23.2	0.2	j
TYC 8557-1251-1	07:55:31.6	-54:36:51	3	15.2 24.6 21.59	0.10 1.0 0.37	j
TYC 8570-1980-1	08:11:09.3	-55:55:56	3	21.8 21.47	0.3 0.36	j
CP-541712	08:37:10.9	-55:18:10	4	20.9	0.24	
CD-612010	08:42:00.4	-62:18:26	4	21.65 22.5	0.58 2.1	j
CD-75392	08:50:05.4	-75:54:38	3	17.41	0.49	
TYC 8590-1193-1	08:56:31.5	-57:00:41	3	19.49	1.97	
TYC 8582-3040-1	08:57:45.6	-54:08:37	4	22.12 22.5	0.36 0.0	j
CD-494008	08:57:52.2	-49:41:51	4	22.03 23.0	0.17 0.2	j
CP-551885	09:00:03.4	-55:38:24	2	25.8	2.55	
CD-552543	09:09:29.3	-55:38:27	4	23.1 22.11 22.5	1.0 0.86 1.0	j
TYC 8174-1586-1	09:11:15.6	-50:14:16	3	22.52 22.5	0.35 1.0	j
CD-542644	09:13:16.9	-55:29:03	2	21.15	0.49	
CP-621293	09:43:08.8	-63:13:04	4	20.91 21.8	0.55 0.1	j
TYC 8946-872-1*	09:55:15.1	-62:03:32	2	21.8	0.31	
TYC 9217-417-1	09:59:57.7	-72:21:47	3	16.95 17.0	0.24 0.4	j
TYC 8962-1747-1	11:08:07.9	-63:41:47	3	17.63 19.3	1.5 1.0	j
HD 107722	12:23:29.0	-77:40:51	3	12.5	0.27	
TYC 460-624-1*	18:45:10.3	+06:20:16	2	-25.2	0.21	
HD 189285*	19:59:24.1	-04:32:06	1	-19.41	0.89	
HD 221451*	23:32:19.2	-13:37:18	2	-6.39	0.86	
Columba members						
CD-52381	01:52:14.6	-52:19:33	7	13.81	0.38	
BD-16351	02:01:35.6	-16:10:01	3	10.03 13.4	0.36 1.9	
CD-44753	02:30:32.4	-43:42:23	2	15.17	2.12	
TYC 8862-19-1	02:58:04.0	-62:41:14	6	16.8 16.6	0.49 0.5	j
BD-11648	03:21:49.7	-10:52:18	2	15.12	0.54	
BD-04700	03:57:37.2	-04:16:16	3	18.28	0.46	
BD-15705*	04:02:16.5	-15:21:30	4	15.14	0.14	
HD 26980	04:14:22.5	-38:19:02	5	21.3 20.2	0.44 0.3	j
HD 27679	04:21:10.3	-24:32:21	2	21.5	0.16	
CD-431395	04:21:48.7	-43:17:33	4	21.68 22.0	0.35 1.0	j
CD-361785	04:34:50.8	-35:47:21	4	22.18 23.3	0.35 1.0	j
GSC 08077-01788	04:51:53.0	-46:47:31	2	17.6	0.76	

ID	RA	DEC	N. of Obs.	RV (km s ⁻¹)	$\sigma^{1,2}$	Reference ³
HD 31242N	04:51:53.5	-46:47:13	2	23.0 -6.9	1.0 4.1	j v
HD 272836	04:53:05.2	-48:44:39	1	22.0 22.81 24.0	0.23 0.89 1.0	
TYC 5900-1180-1*	04:58:35.8	-15:37:31	1	23.56	0.89	
BD-08995	04:58:48.6	-08:43:40	3	24.08	0.52	
HD 32372	05:00:51.9	-41:01:07	2	23.17	0.29	
HD 274561	05:28:55.1	-45:34:58	2	24.57	0.16	
BD-191194	05:30:19.1	-19:16:32	1	26.16	0.89	
CD-392075*	05:37:05.3	-39:32:26	3	23.06 23.1	0.29 0.6	j
BD-081195	05:38:35.0	-08:56:40	4	24.16 26.2	0.58 -	
CD-382198	05:45:16.3	-38:36:49	4	26.87	0.71	
CD-292531	05:50:21.4	-29:15:21	3	26.54 27.5	0.38 1.0	j
HD 40216	05:55:43.1	-38:06:16	2	24.38	0.09	
AB Pic	06:19:12.9	-58:03:16	6	22.94 22.6	0.34 0.3	j
CD-402458	06:26:06.9	-41:02:54	4	25.59 25.0	0.45 1.0	j
HD 48370	06:43:01.0	-02:53:19	1	23.38	0.89	
CD-363202	06:52:46.8	-36:36:17	1	5.22 25.6	0.89 1.0	j
TYC 9178-284-1	06:55:25.2	-68:06:21	3	20.09 20.1	0.16 0.1	j
HD 51797	06:56:23.5	-46:46:55	5	25.2 25.2	0.31 0.2	j
HD 55279	07:00:30.5	-79:41:46	3	17.59	0.15	
CP-531875*	08:45:52.7	-53:27:28	1	21.82	0.89	
V479 Car	09:23:34.9	-61:11:36	5	23.2 20.82	1.0 0.15	j
CP-522481	09:32:26.1	-52:37:40	6	20.8 21.37	0.4 0.56	j
HD 298936	10:13:14.6	-52:30:54	4	17.71 17.7	0.28 1.0	j
CD-544320*	11:45:51.8	-55:20:46	4	16.01	0.41	

 ϵ -Chamaeleon members

EG Cha	08:36:56.2	-78:56:46	3	18.22 18.4	0.72 1.0	j
EO Cha	08:44:31.9	-78:46:31	3	17.32 15.0	0.11 -	
EQ Cha*	08:47:56.8	-78:54:53	3	22.98 18.0	0.77 -	
1RXS J091528.1-760856	09:15:29.1	-76:08:47	3	19.1 21.0	0.55 2.0	
1RXS J093455.3-780414	09:34:56.1	-78:04:19	3	16.77	0.61	
1RXS J100515.1-774900	10:05:20.0	-77:48:42	3	16.38	0.06	
DZ Cha	11:49:31.9	-78:51:01	3	14.02 18.0	0.42 -	
T Cha	11:57:13.5	-79:21:32	1	14.71	0.89	
GSC 09415-02676*	11:58:26.9	-77:54:45	3	14.47	0.24	

ID	RA	DEC	N. of Obs.	RV (km s ⁻¹)	$\sigma^{1,2}$	Reference ³
HIP 58490	11:59:42.3	-76:01:26	5	13.0 13.66 15.1	2.2 0.51 1.0	o j
DX Cha	12:00:05.1	-78:11:35	2	11.51	0.36	
HD 104237-5	12:00:08.3	-78:11:40	2	13.7	0.03	
HD 104237-6	12:00:09.3	-78:11:42	3	13.76	1.41	
HD 104467	12:01:39.1	-78:59:17	5	13.32 12.3 15.4	3.07 1.4 1.0	j g
GSC 09420- 00948	12:02:03.8	-78:53:01	4	12.66 17.1 5.0	3.23 -	e e
HD 105923	12:11:38.1	-71:10:36	5	14.2 14.2	0.37 1.0	j
1RXS J121645.2-775339	12:16:46.0	-77:53:33	4	14.03 14.0	0.18 2	o
G92391495	12:19:43.8	-74:03:57	3	13.92	0.08	
GSC 09239-01572	12:20:21.9	-74:07:39	4	12.65	3.26	
CD-74712	12:39:21.3	-75:02:39	9	13.31 14.4	0.34 0.2	j
CD-691055	12:58:25.6	-70:28:49	3	12.35 12.8 11.1	0.7 1.0 1.5	j r
CP-681894	13:22:07.5	-69:38:12	6	11.66 11.6	0.76 0.2	j

Octans members

CD-58860	04:11:55.6	-58:01:47	4	9.52 9.8	0.06 1.0	j
CD-431451	04:30:27.3	-42:48:47	5	13.17	0.38	
HD 274576	05:28:51.4	-46:28:19	4	12.05 12.7	0.66 1.0	
BD-201111	05:32:29.3	-20:43:33	2	19.36	0.23	
CD-471999	05:43:32.1	-47:41:11	2	11.67 14.4	2.28 1.0	j
TYC 7066-1037-1	05:58:11.8	-35:00:49	4	14.52	0.25	
CD-492037	06:03:35.4	-49:11:26	5	12.12	0.19	
CD-303394N	06:40:04.9	-30:33:03	4	14.51	0.17	
CD-303394S	06:40:05.7	-30:33:09	2	14.87	1.1	
TYC 9300-529-1	18:49:45.1	-71:56:58	3	-2.26	0.47	
CP-82784	19:53:56.7	-82:40:42	1	-2.15 -2.0	0.89 1.2	j
CD-87121	23:58:17.7	-86:26:24	6	-0.86	1.41	

Tucana Horologium members

HD 105	00:05:52.5	-41:45:11	1	2.05 3.2	0.89 1.3	a
HD 987	00:13:52.8	-74:41:17	6	9.78 8.8	0.45 0.3	f
HD 1466	00:18:26.1	-63:28:39	4	6.23	0.18	
HIP 1993	00:25:14.7	-61:30:48	1	6.06	0.89	
CD-7824	00:42:20.3	-77:47:40	7	11.87 11.5	0.51 0.6	j

ID	RA	DEC	N. of Obs.	RV (km s ⁻¹)	$\sigma^{1,2}$	Reference ³
HD 8558	01:23:21.1	-57:28:50	8	9.56	0.36	
				8.3	0.4	g
HD 9054	01:28:08.6	-52:38:19	3	8.55	0.2	
HD 12039	01:57:49.0	-21:54:05	2	5.83	0.38	
				5.8	0.4	f
HD 13183	02:07:17.9	-53:11:56	11	9.87	0.4	
				9.7	0.3	f
				9.5	0.2	g
HD 13246	02:07:26.1	-59:40:46	6	9.79	0.48	
CD-60416	02:07:32.1	-59:40:21	5	10.59	0.74	
GSC 08491-01194	02:41:47.3	-52:59:31	1	12.85	0.89	
				12.5	1.2	j
CD-58553	02:42:33.0	-57:39:37	5	12.54	0.4	
				12.4	0.1	j
CD-351167	03:19:08.6	-35:07:00	3	13.57	0.11	
				13.5	0.2	j
CD-461064	03:30:49.1	-45:55:57	1	14.06	0.89	
				15.3	0.5	j
CD-441173	03:31:55.6	-43:59:14	6	15.65	0.36	
				15.5	0.3	j
HD 22705	03:36:53.4	-49:57:29	4	14.34	1.51	
HD 24636	03:48:11.5	-74:41:39	3	13.69	0.56	
BD-12943	04:36:47.1	-12:09:21	2	17.31	0.41	
HD 29615	04:38:43.9	-27:02:02	4	18.92	0.32	
HD 30051*	04:43:17.2	-23:37:42	3	-2.03	0.50	
TYC 8083-455-1	04:48:00.7	-50:41:26	3	18.91	0.2	
				19.3	0.1	j
BD-191062	04:59:32.0	-19:17:42	3	20.12	0.44	
BD-091108	05:15:36.5	-09:30:51	4	20.8	0.34	
				21.0	-	t
CD-302310	05:18:29.0	-30:01:32	4	20.99	0.53	
TYC 8098-414-1	05:33:25.6	-51:17:13	2	18.51	1.52	
				20.5	0.0	j
CD-272520	05:49:06.6	-27:33:56	2	23.0	0.43	
HD 47875	06:34:41.0	-69:53:06	5	15.75	1.92	
GSC 09507-02466*	11:40:16.5	-83:21:00	3	13.06	0.37	
				13.4	0.8	j
HD 202917	21:20:50.0	-53:02:03	6	-1.16	0.39	
				0.1	0.2	f
				-1.6	0.2	g
				-5.3	-	i
				-0.9	0.7	j
				-0.9	A	n
HIP 107345	21:44:30.1	-60:58:39	3	2.09	0.4	
				2.3	0.5	j
HD 207575	21:52:09.7	-62:03:09	3	1.57	0.17	
HD 222259N	23:39:39.1	-69:11:39	6	6.21	0.32	
				7.4	0.2	g
				6.1	0.1	j
				8.3	A	n
HD 222259S	23:39:39.3	-69:11:44	8	7.9	0.17	

TW Hyrae members

TWA 7	10:42:30.1	-33:40:17	2	11.89	0.37	
TW Hya	11:01:51.9	-34:42:17	2	12.45	0.52	
				13.4	0.8	j

ID	RA	DEC	N. of Obs.	RV (km s ⁻¹)	$\sigma^{1,2}$	Reference ³
CD-298887	11:09:13.8	-30:01:40	2	10.98	0.03	
				12.1	1.0	j
TWA 12	11:21:05.5	-38:45:16	2	10.85	0.33	
CD-347390A*	11:21:17.2	-34:46:46	4	10.8	0.43	
				11.3	1.0	j
CD-347390B*	11:21:17.4	-34:46:50	4	11.48	0.4	
				11.6	1.0	j
CD-268632A	11:32:41.2	-26:51:56	2	8.06	0.43	
				8.0	1.0	j
TWA 9B	11:48:23.7	-37:28:49	1	11.51	0.89	
				9.5	B	n
TWA 9A	11:48:24.2	-37:28:49	3	10.39	0.62	
TWA 23	12:07:27.4	-32:47:00	2	10.93	0.1	
CD-397538	12:15:30.7	-39:48:43	3	7.03	0.58	
TWA 16	12:34:56.4	-45:38:07	3	8.74	0.36	
				9.0	-	t
TWA 10	12:35:04.2	-41:36:39	3	6.31	0.23	
				6.6	1.0	j

(*) No longer classified as a member of association with new RV values.

(a) RV values from a single-component Gaussian fit; see Section B.4 for details on target.

(1) Uncertainties for UVES and FEROS data: If more than one observation was available uncertainties were taken to be the standard deviation from the mean value for each target. If there was only one observation the uncertainty has a value of 0.89 km s⁻¹, one standard deviation of the entire sample.

(2) Uncertainties from [de Bruijne & Eilers \(2012\)](#) have values (A): the standard errors are generally reliable or (B): potential, small, uncorrected, systematic errors.

(3) **References:** a: I/196 ([Turon et al. 1993](#)), b: I/306A/ ([Ivanov 2008](#)), c:III/105/ ([Andersen et al. 1985](#)), d: III/198/ ([Reid et al. 1995](#)), e: III/249/ ([Malaroda et al. 2006](#)), f: III/252 ([Gontcharov 2006](#)), g: III/254/ ([Kharchenko et al. 2007](#)), h: III/265/ ([Siebert et al. 2011](#)), i :J/A+A/423/517/ ([Rocha-Pinto et al. 2004](#)), j: J/A+A/460/695/ ([Torres et al. 2006](#)), k: J/A+A/521/A12/ ([Maldonado et al. 2010](#)), l: J/A+A/530/A138/ ([Casagrande et al. 2011](#)), m: J/A+A/531/A8/ ([Jenkins et al. 2011](#)), n: J/A+A/546/A61/ ([de Bruijne & Eilers 2012](#)), o: J/A+A/551/A46/ ([Lopez Martí et al. 2013](#)), p: J/A+AS/142/275/ ([Strassmeier et al. 2000](#)), q: J/AJ/133/2524/ ([White et al. 2007](#)), r: J/AJ/144/8/ ([Song et al. 2012](#)), s: J/AZh/83/821/ ([Bobylev et al. 2006](#)), t: J/AcA/62/67/ ([Kiraga 2012](#)), u: V/137D/XHIP ([Anderson & Francis 2012](#)), v: III/272/ ([Kordopatis et al. 2013](#)).

Table C.2. Summary table of UVES radial velocity values for SB2 and SB3 systems.

ID	RA	DEC	MJD	Ass.	Flux Ratio	RV ₁	σ_1	RV ₂	σ_2	RV ₃	σ_3
BD-20951	04:52:49.5	-19:55:02	56125.4 56139.4	CAR	0.25	-27.1 -27.5	0.1 0.9	80.2 81.9	0.2 0.9		
HD 33999	05:12:35.8	-34:28:48	55410.4	ABD	0.70, 0.20	28.7	0.5	-15.7	0.2	59.0	1.0
HD 309751	09:31:44.7	-65:14:53	55885.3	CAR	0.48	-7.4	0.3	53.0	0.6		
TWA 20*	12:31:38.1	-45:58:59	56054.2 56069.2 56111.1	TWA	0.79	-50.5 -47.5 -47.8	1.8 1.5 1.2	76.1 72.5 71.7	2.3 1.4 1.6		
HD 155177	17:42:09.0	-86:08:05	54209.4 54765.0 56056.4 56092.3	OCT	0.86	12.2 7.4 -17.2 15.4	0.3 0.9 0.1 0.5	-21.9 -7.0 31.3 -7.6	0.6 0.7 0.3 0.5		
V4046-Sgr	18:14:10.5	-32:47:33	53600.0 54237.4 54238.1 54238.3 54235.3 54238.4 54239.4 54237.1 54239.2 53597.1 54239.1 54235.4 54237.2 54235.2 54238.2 53597.0 53598.0 53599.0	BPC	0.77	-21.0 -59.9 -12.3 -31.8 -53.8 -43.4 -17.6 -37.7 -22.2 -58.4 -32.9 -43.4 -49.3 -59.8 -20.0 -58.0 -51.0 -20.0	0.5 0.2 1.3 0.2 0.3 0.1 0.4 0.3 0.1 0.2 0.3 2.9 0.1 0.1 10.1 0.3 0.2 0.2 0.1	9.3 44.1 -1.8 20.6 38.8 34.4 2.2 23.1 9.5 47.7 20.3 29.2 34.0 43.3 10.1 47.2 35.4 10.2	0.7 0.1 1.0 0.3 0.1 0.0 0.2 0.1 0.3 0.2 0.3 2.8 0.1 0.1 0.1 0.2 0.8 0.3		
1RXS J195602.8-320720	19:56:02.9	-32:07:19	55843.1	BPC	0.67	30.0	0.4	-46.2	0.4		
HD 217379	23:00:28.0	-26:18:43	55341.4	ABD	0.62, 0.30	50.0	0.4	-49.7	0.1	5.5	0.4
CD-423328	07:33:21.2	-42:55:42	56175.4 56179.4	CAR	1.00 ^a	36.0 33.5	0.6 0.4	11.2 12.5	0.5 0.5		

(*) No longer classified as a member of association with new RV values.

(^a) From CCF profiles in both epochs, it is difficult to accurately compute the flux ratio; however, the two components are very similar, and thus, we assign a value of 1.00.

Table C.3. RV values from each UVES observation available.

ID	RA	DEC	MJD	RV (km s ⁻¹)	$\pm\sigma_{meas.}$
AB Doradus members					
HD 6569	01:06:26.2	-14:17:47	54749.10	7.6	.004
			55391.42	7.5	.003
BD-12243	01:20:32.3	-11:28:04	54281.37	9.9	.003
			55391.41	10.6	.003
HD 16760B	02:42:21.0	+38:37:21	55415.40	-3.5	.004
HD 16760	02:42:21.3	+38:37:07	55415.40	-3.2	.004
HD 17332B	02:47:27.2	+19:22:21	55415.41	5.1	.003
HD 17332A	02:47:27.4	+19:22:19	55415.41	3.9	.009
IS Eri	03:09:42.3	-09:34:47	54749.14	14.3	.006
			55391.43	14.6	.004
HD 24681	03:55:20.4	-01:43:45	54795.03	18.0	.022
HD 25457	04:02:36.7	-00:16:08	54795.03	18.0	.028
			55391.42	17.3	.020
HD 31652	04:57:22.3	-09:08:00	54784.13	22.6	.004
CD-401701	05:02:30.4	-39:59:13	54309.40	28.6	.003
			55410.38	28.6	.004
HD 32981	05:06:27.7	-15:49:30	55458.30	25.6	.005
HD 293857	05:11:09.7	-04:10:54	54808.11	20.3	.006
HD 35650	05:24:30.2	-38:58:11	54784.25	31.4	.004
			55410.40	32.7	.005
CD-342331	05:35:04.1	-34:17:52	54805.24	30.7	.015
			55410.41	30.4	.015
CD-481893	05:36:55.1	-47:57:48	54805.17	31.7	.016
			55459.25	32.0	.017
UY Pic	05:36:56.9	-47:57:53	54309.41	32.2	.006
			54327.41	32.1	.004
			55459.25	32.6	.006
WX Col	05:37:12.9	-42:42:56	54312.40	31.3	.004
			55398.42	31.2	.019
			55459.25	31.3	.005
TYC 7604-1675-1	05:37:13.2	-42:42:57	54309.42	30.3	.003
TYC 4779-394-1	05:38:56.6	-06:24:41	54814.09	22.9	.005
CP-19878	05:39:23.2	-19:33:29	55416.42	28.7	.025
TYC 7605-1429-1	05:41:14.3	-41:17:59	55461.36	30.7	.145
TZ Col	05:52:16.0	-28:39:25	54814.11	29.0	.024
			55463.25	28.5	.020
BD-131328	06:02:21.9	-13:55:33	54878.03	25.4	.004
CD-342676	06:08:33.9	-34:02:55	54226.97	29.8	.006
			55464.25	30.6	.009
CD-352722	06:09:19.2	-35:49:31	54805.34	31.9	.015
HD 45270	06:22:30.9	-60:13:07	54228.98	31.8	.018
			54805.21	31.5	.015
			55465.36	31.2	.011
AK Pic	06:38:00.4	-61:32:00	55466.36	36.8	.021
CD-611439	06:39:50.0	-61:28:42	54805.18	31.4	.005
TYC 7627-2190-1	06:41:18.5	-38:20:36	54896.09	25.6	.049
			55416.40	27.2	.063
GSC 08544-01037*	06:47:53.4	-57:13:32	54773.34	29.6	.005
			55468.33	29.8	.003
CD-571654	07:10:50.6	-57:36:46	54876.22	29.3	.032
			55464.38	29.0	.050
V429 Gem	07:23:43.6	+20:24:59	54893.08	7.0	.006

ID	RA	DEC	MJD	RV (km s ⁻¹)	$\pm\sigma_{meas.}$
			55468.38	7.8	.006
HD 59169	07:26:17.7	-49:40:51	55468.39	39.7	.008
CD-8480	07:30:59.5	-84:19:28	54236.98	23.2	.003
HD 64982	07:45:35.6	-79:40:08	54239.99	25.6	.012
			55464.38	25.7	.011
BD+012447	10:28:55.5	+00:50:28	54850.37	7.7	.008
PX Vir	13:03:49.7	-05:09:43	54888.38	-13.3	.004
HD 139751	15:40:28.4	-18:41:46	55340.14	-7.6	.006
HIP 81084	16:33:41.6	-09:33:12	54923.41	-14.7	.005
HD 152555	16:54:08.1	-04:20:25	54906.34	-16.4	.015
			55341.29	-16.5	.018
HD 178085	19:10:57.9	-60:16:20	55341.31	8.4	.030
TYC 486-4943-1	19:33:03.8	+03:45:40	55339.41	-20.7	.004
BD-034778	20:04:49.4	-02:39:20	54783.00	-16.5	.006
			55340.40	-16.5	.006
HD 199058	20:54:21.1	+09:02:24	54783.00	-19.4	.006
			55340.40	-19.7	.011
TYC 1090-543-1	20:54:28.0	+09:06:07	54783.01	-19.0	.012
			55339.41	-19.3	.013
HD 201919	21:13:05.3	-17:29:13	54783.02	-7.5	.005
			55340.40	-7.6	.005
HD 218860	23:11:52.0	-45:08:10	54227.41	9.6	.004
			54760.26	12.7	.004
HD 224228	23:56:10.7	-39:03:08	55341.41	13.1	.004

Argus members

CD-292360	05:34:59.2	-29:54:04	54309.41	25.7	.006
			56139.39	26.1	.020
			56140.41	25.3	.011
CD-283434	06:49:45.4	-28:59:17	54234.97	26.7	.004
CD-422906	07:01:53.4	-42:27:56	54234.99	23.4	.004
			56159.40	23.7	.014
			56163.38	23.8	.015
HD 61005	07:35:47.5	-32:12:14	56175.40	22.2	.010
			56179.38	22.6	.013
CD-483199	07:47:26.0	-49:02:51	54876.23	17.8	.037
			54878.04	17.6	.025
			56175.39	17.1	.052
			56179.39	17.9	.025
CD-433604	07:48:49.8	-43:27:06	54876.23	20.4	.056
			56175.38	24.1	.142
			56179.37	11.0	.010
TYC 8561-970-1	07:53:55.5	-57:10:07	54232.01	15.7	.003
			56082.01	15.9	.010
			56162.39	15.7	.008
PMM 7956	08:29:51.9	-51:40:40	54876.26	16.1	.007
PMM 6974	08:34:18.1	-52:15:58	54864.29	15.1	.004
PMM 4280	08:34:20.5	-52:50:05	54876.27	16.9	.022
PMM 6978	08:35:01.2	-52:14:01	54876.28	15.4	.006
PMM 3359	08:36:55.0	-53:08:34	54876.29	14.7	.010
PMM 665	08:37:51.6	-53:45:46	54876.31	14.6	.010
PMM 4362	08:38:22.9	-52:56:48	54876.35	15.1	.017
PMM 686	08:39:22.6	-53:55:06	54880.12	15.2	.007
V364 Vel	08:39:53.0	-52:57:57	54880.14	15.3	.013

ID	RA	DEC	MJD	RV (km s ⁻¹)	$\pm\sigma_{meas.}$
PMM 8415	08:40:16.3	-52:56:29	54880.16	14.8	.017
PMM 1142	08:40:49.1	-53:37:45	54878.04	14.1	.006
PMM 756	08:43:00.4	-53:54:08	54878.05	16.1	.012
V376 Vel	08:44:05.2	-52:53:17	54878.06	13.6	.015
V379 Vel	08:45:26.9	-52:52:02	54864.27	14.7	.005
CD-572315	08:50:08.1	-57:45:59	54893.10	13.4	.017
TYC 8594-58-1	09:02:03.9	-58:08:50	54880.18 56082.02 56108.00	10.8 8.2 10.9	.036 .088 .068
CD-542644	09:13:16.9	-55:29:03	54898.17 55885.32	20.8 21.5	.037 .095
BD-202977	09:39:51.4	-21:34:17	54240.09	17.9	.005
TYC 9217-641-1	09:42:47.4	-72:39:50	54880.20	5.4	.014
CD-395833	09:47:19.9	-40:03:10	54240.01 56097.96	14.8 14.5	.004 .011
HD 309851	09:55:58.3	-67:21:22	54227.14 54895.22 56097.98	7.3 7.1 8.0	.012 .020 .032
CD-74673	12:20:34.4	-75:39:29	54874.28	4.7	.004
CD-75652	13:49:12.9	-75:49:48	54226.13 54883.33 56134.09 56137.13	-1.0 -1.2 -0.9 -1.4	.063 .016 .014 .031
NY Aps	15:12:23.4	-75:15:16	54905.22 56033.40	-3.1 -3.5	.009 .017

 β -Pic members

HIP 10679	02:17:24.7	+28:44:30	54805.16	5.3	.007
BD+05378*	02:41:25.9	+05:59:18	54788.24	7.3	.005
GJ3305*	04:37:37.5	-02:29:28	55846.23 55925.24 55935.13	24.4 23.3 23.8	.038 .014 .017
V1005Ori	04:59:34.8	+01:47:01	54808.10 55846.30 55925.24	18.8 19.4 18.6	.013 .008 .019
CD-571054	05:00:47.1	-57:15:25	54773.29	19.0	.007
BD-211074B	05:06:49.5	-21:35:04	55846.25 55847.27 55904.19	21.8 22.0 20.8	.034 .025 .017
BD-211074A	05:06:49.9	-21:35:09	55846.26 55855.36 55904.19	21.5 20.9 20.8	.013 .017 .017
TYC 112-917-1	05:20:00.3	+06:13:04	55846.26 55925.24 55935.15	19.0 18.7 18.7	.009 .010 .011
TYC 112-1486-1	05:20:31.8	+06:16:11	55846.27 55925.25 55936.21	18.4 18.8 18.3	.020 .024 .017
V1311 Ori*	05:32:04.5	-03:05:29	54784.35 55846.28 55904.18	23.9 24.5 23.2	.020 .020 .021
AO Men	06:18:28.2	-72:02:41	54805.18 55846.30 55855.35 54226.99	16.1 16.5 16.0 16.0	.009 .026 .018 .007
TWA 22	10:17:26.9	-53:54:27	55904.30	13.4	.057

ID	RA	DEC	MJD	RV (km s ⁻¹)	$\pm\sigma_{meas.}$
HD 139084B	15:38:56.8	-57:42:19	55968.36	13.6	.051
V343 Nor	15:38:57.5	-57:42:27	55978.37 54226.24 54906.32	3.0 5.0 0.2	.187 .007 .010
CD-2711535	17:15:03.6	-27:49:40	55845.05	-8.3	.013
CD-547336	17:29:55.1	-54:15:49	54905.23	1.5	.043
HD 164249	18:03:03.4	-51:38:56	54209.40	-0.7	.017
GSC 07396-00759	18:14:22.1	-32:46:10	55843.05	-6.0	.021
TYC 9073-762-1	18:46:52.6	-62:10:36	55843.06	1.6	.024
CD-2613904	19:11:44.7	-26:04:09	55843.07	-9.7	.011
HD 181327	19:22:58.9	-54:32:17	54226.33 55843.08 55850.07	-1.0 -0.8 -0.3	.016 .034 .051
TYC 7443-1102-1	19:56:04.4	-32:07:38	55843.09 55850.07	-6.4 -6.3	.010 .018
1RXS J200136.9-331307	20:01:37.2	-33:13:14	55843.10 55850.08 56009.36	-4.6 -4.4 -5.0	.017 .010 .015
AU Mic	20:45:09.5	-31:20:27	54765.05 55844.10 53608.97	-5.1 -5.2 -4.9	.018 .010 .121
AZ Cap	20:56:02.7	-17:10:54	55843.11 55889.03	-8.2 -8.5	.017 .020
CP-722713	22:42:48.9	-71:42:21	54765.07	7.8	.006
WW PsA	22:44:58.0	-33:15:02	55843.11 55850.09	1.1 1.6	.046 .074
TX PsA	22:45:00.0	-33:15:26	55850.10	2.7	.277
BD-136424	23:32:30.9	-12:15:52	54760.25 55889.06	0.7 0.2	.009 .018

Carina members

HD 269620	05:29:27.1	-68:52:05	54228.97	19.1	.013
HD 42270	05:53:29.3	-81:56:53	54805.20	16.9	.033
HD 49855*	06:43:46.2	-71:58:35	54805.19	20.8	.011
CD-571709	07:21:23.7	-57:20:37	54215.00 55849.31	23.2 22.9	.005 .019
CD-423328 ^a	07:33:21.2	-42:55:42	56175.40 56179.38	15.1 15.3	.130 .110
TYC 8557-1251-1	07:55:31.6	-54:36:51	55856.32	21.1	.039
TYC 8570-1980-1	08:11:09.3	-55:55:56	55856.32	21.3	.052
CP-541712	08:37:10.9	-55:18:10	54233.02 55849.33	20.7 20.7	.013 .038
CD-612010	08:42:00.5	-62:18:26	54897.17 55856.33	21.0 22.1	.041 .158
TYC 8590-1193-1	08:56:31.5	-57:00:41	55885.29 55910.18	21.0 20.8	.012 .010
TYC 8582-3040-1	08:57:45.6	-54:08:37	54897.18 55885.29	21.7 21.8	.033 .015
CD-494008	08:57:52.2	-49:41:51	54898.15 55885.30	22.1 21.8	.065 .032
CP-551885	09:00:03.4	-55:38:24	54898.16 55885.31	27.6 24.0	.078 .185
CD-552543	09:09:29.4	-55:38:27	54233.03 55885.31 55910.20	20.6 22.6 22.4	.015 .014 .008
TYC 8174-1586-1	09:11:15.8	-50:14:15	55885.31	22.2	.023

ID	RA	DEC	MJD	RV (km s ⁻¹)	$\pm\sigma_{meas.}$
CP-621293	09:43:08.8	-63:13:04	55909.30 54898.19 55885.34	22.4 20.6 20.4	.021 .073 .036
TYC 8946-872-1*	09:55:15.1	-62:03:32	55909.30 55933.28	22.1 21.5	.022 .019
TYC 9217-417-1	09:59:57.7	-72:21:47	55933.29	16.6	.034
TYC 8962-1747-1	11:08:07.9	-63:41:47	55935.30 55981.23	16.3 16.8	.011 .010
HD 107722	12:23:29.0	-77:40:51	54906.29 55978.35 55981.25	12.8 12.5 12.2	.056 .100 .231
TYC 460-624-1*	18:45:10.3	+06:20:16	55843.06 56009.35	-25.0 -25.4	.020 .018
HD 189285*	19:59:24.1	-04:32:06	55340.39	-19.4	.007
HD 221451*	23:32:19.2	-13:37:18	55889.06	-7.3	.010
Columba members					
CD-52381	01:52:14.6	-52:19:33	54254.36 54258.42 54750.14	13.7 13.5 13.4	.011 .023 .010
BD-16351	02:01:35.6	-16:10:01	54749.11 56107.42 56116.38	10.5 9.7 9.9	.009 .008 .009
CD-44753	02:30:32.4	-43:42:23	54749.12	13.1	.007
TYC 8862-19-1	02:58:04.0	-62:41:14	54281.38	16.2	.004
BD-11648	03:21:49.7	-10:52:18	56125.36 56141.35	14.6 15.7	.040 .045
BD-04700	03:57:37.2	-04:16:16	54755.16 56125.37 56128.42	18.4 18.8 17.7	.014 .010 .024
BD-15705*	04:02:16.5	-15:21:30	54765.11 56108.42 56119.42	15.0 15.2 15.3	.008 .011 .007
			56125.37	15.0	.006
HD 26980	04:14:22.6	-38:19:02	54288.42 54308.42	21.3 21.4	.016 .007
HD 27679	04:21:10.3	-24:32:21	54288.41 54784.11	21.3 21.7	.008 .009
CD-431395	04:21:48.7	-43:17:33	54784.12 56125.38 56138.33	22.2 21.8 21.2	.046 .019 .042
CD-361785	04:34:50.8	-35:47:21	56125.38 56138.34 54308.40	21.7 22.5 22.1	.012 .010 .003
GSC 08077-01788	04:51:53.0	-46:47:31	54772.23 54773.30	18.4 16.8	.023 .011
HD 31242N	04:51:53.5	-46:47:13	54309.39 54772.21	22.2 21.8	.010 .021
HD 272836	04:53:05.2	-48:44:39	54772.22	22.8	.010
TYC 5900-1180-1*	04:58:35.8	-15:37:31	54784.14	23.6	.024
BD-08995	04:58:48.6	-08:43:40	54795.04 56144.41	24.7 23.5	.010 .007
			56147.39	24.0	.010
HD 32372	05:00:51.9	-41:01:07	54309.39	22.9	.005
HD 274561	05:28:55.1	-45:34:58	54307.41	24.4	.003
BD-191194	05:30:19.1	-19:16:32	54784.25	26.2	.019
CD-392075*	05:37:05.3	-39:32:26	54312.40	23.2	.010
BD-081195	05:38:35.0	-08:56:40	54814.08	24.1	.060

ID	RA	DEC	MJD	RV (km s ⁻¹)	$\pm\sigma_{meas.}$
CD-382198	05:45:16.3	-38:36:49	56144.41	23.2	.029
			56147.40	24.6	.077
			56159.41	24.7	.059
			54814.10	25.7	.017
CD-292531	05:50:21.4	-29:15:21	56139.39	27.4	.045
			56140.42	27.4	.041
HD 40216	05:55:43.2	-38:06:16	56140.41	26.1	.013
			54814.12	24.5	.054
AB Pic	06:19:12.9	-58:03:16	54226.99	22.8	.004
CD-402458	06:26:06.9	-41:02:54	54327.40	25.7	.019
			56144.42	25.1	.006
HD 48370	06:43:01.0	-02:53:19	56147.40	25.3	.018
			54807.35	23.4	.006
TYC 9178-284-1	06:55:25.2	-68:06:21	54214.98	19.9	.004
HD 51797	06:56:23.5	-46:46:55	54234.98	24.9	.011
			54805.34	25.0	.006
HD 55279	07:00:30.5	-79:41:46	54214.02	17.4	.004
			54239.98	20.6	.012
V479 Car	09:23:35.0	-61:11:36	55885.33	20.8	.004
			54843.22	20.7	.007
CP-522481	09:32:26.1	-52:37:40	54240.00	20.9	.008
			54240.00	20.8	.024
HD 298936	10:13:14.8	-52:30:54	54898.18	21.0	.009
			55885.33	21.5	.012
CD-544320*	11:45:51.8	-55:20:46	54223.08	17.8	.009
			55862.36	17.8	.003
CD-544320*	11:45:51.8	-55:20:46	55933.31	17.2	.010
			54884.24	16.2	.003
CD-544320*	11:45:51.8	-55:20:46	55935.30	16.2	.006
			55981.31	15.3	.005

 ϵ Chamaeleon members

EG Cha	08:36:56.2	-78:56:46	55849.32	17.3	.029
EO Cha	08:44:31.9	-78:46:31	55856.36	19.1	.026
			55910.23	17.4	.014
EQ Cha*	08:47:56.8	-78:54:53	55932.29	17.4	.011
			55933.22	17.2	.019
1RXS J091528.1-760856	09:15:29.1	-76:08:47	55910.17	24.0	.049
			55932.30	22.2	.067
1RXS J093455.3-780414	09:34:56.1	-78:04:19	55933.24	22.8	.083
			55910.29	19.1	.020
1RXS J100515.1-774900	10:05:20.0	-77:48:42	55933.25	18.4	.020
			55936.23	19.8	.031
DZ Cha	11:49:31.9	-78:51:01	55910.28	16.0	.069
			55933.27	17.5	.072
T Cha	11:57:13.5	-79:21:32	55981.21	16.7	.034
			55910.30	16.4	.019
GSC 09415-02676*	11:58:26.9	-77:54:45	55933.30	16.3	.021
			55981.23	16.4	.024
GSC 09415-02676*	11:58:26.9	-77:54:45	55935.31	14.0	.020
			55981.30	14.5	.020
GSC 09415-02676*	11:58:26.9	-77:54:45	55993.17	13.5	.018
			56049.17	14.7	.028
GSC 09415-02676*	11:58:26.9	-77:54:45	55935.32	14.8	.041
			55977.27	14.4	.017
GSC 09415-02676*	11:58:26.9	-77:54:45	55993.19	14.2	.016

ID	RA	DEC	MJD	RV (km s ⁻¹)	$\pm\sigma_{meas.}$
HIP 58490	11:59:42.3	-76:01:26	54901.15	14.5	.011
			55340.07	13.6	.009
			55981.25	13.8	.006
			55993.20	13.0	.012
			56009.34	13.3	.011
DX Cha	12:00:05.1	-78:11:35	52663.37	11.8	.017
HD 104237-5	12:00:08.3	-78:11:40	54463.33	11.9	.013
			55979.36	13.7	.050
			55982.34	13.7	.059
HD 104237-6	12:00:09.3	-78:11:42	55993.21	13.4	.053
			56012.32	15.6	.029
			55340.09	12.2	.055
HD 104467	12:01:39.1	-78:59:17	54906.28	11.0	.027
			55342.12	15.9	.041
			55981.26	10.1	.022
			55993.22	11.5	.051
			53453.23	18.0	.016
GSC 09420- 00948	12:02:03.8	-78:53:01	54901.16	18.2	.031
			55977.29	10.4	.024
			55981.27	11.3	.017
			55982.33	10.7	.024
			54223.12	13.9	.019
HD 105923	12:11:38.1	-71:10:36	55342.12	14.0	.014
			55981.25	13.9	.005
			55982.32	14.2	.007
1RXS J121645.2-775339	12:16:46.0	-77:53:33	55947.36	13.9	.027
			55977.29	14.1	.027
			55979.33	13.8	.020
			55981.28	14.3	.029
			55947.34	14.0	.015
GSC 09239-01495	12:19:43.8	-74:03:57	55979.32	13.9	.009
			55981.32	13.9	.023
			55340.11	16.4	.097
GSC 09239-01572	12:20:21.9	-74:07:39	55947.35	12.0	.180
			55978.34	8.6	.246
			55979.30	13.6	.197
CD-74712	12:39:21.3	-75:02:39	54226.09	13.4	.012
			54906.30	13.9	.021
			55371.07	13.9	.037
			55978.35	13.2	.017
			55982.26	12.9	.041
CD-691055	12:58:25.6	-70:28:49	55978.36	12.5	.032
			55981.31	11.4	.064
CP-681894	13:22:07.5	-69:38:12	54222.19	10.3	.006
			54877.38	12.1	.018
			55398.07	12.3	.027
			55978.36	10.9	.014

Octans members

CD-58860	04:11:55.7	-58:01:47	54765.10	9.6	.035
			56108.42	9.5	.026
			56122.42	9.5	.023
CD-431451	04:30:27.3	-42:48:47	54309.38	12.9	.033
			54765.10	12.6	.010
			56108.41	13.2	.024
			56122.41	13.5	.019
HD 274576	05:28:51.4	-46:28:19	54805.17	12.2	.017
			56125.41	10.9	.043

ID	RA	DEC	MJD	RV (km s ⁻¹)	$\pm\sigma_{meas.}$
BD-201111	05:32:29.3	-20:43:33	56138.37	12.4	.039
			56140.39	19.1	.057
			56144.39	19.6	.048
CD-471999 TYC 7066-1037-1	05:43:32.1 05:58:11.8	-47:41:11 -35:00:49	56140.38	14.0	.071
			54903.11	14.7	.038
			56139.40	14.8	.032
CD-492037	06:03:35.4	-49:11:26	56140.40	14.3	.018
			54214.00	12.3	.004
			54214.00	12.3	.013
CD-303394N	06:40:04.9	-30:33:03	56139.39	12.0	.012
			56140.39	11.8	.003
			54896.08	14.4	.072
CD-303394S TYC 9300-529-1	06:40:05.7 18:49:45.1	-30:33:09 -71:56:58	56159.39	14.4	.185
			56161.40	14.8	.124
			56161.40	16.0	.115
CD-87121	23:58:17.7	-86:26:24	56056.39	-1.6	.054
			56087.39	-2.5	.033
			54242.26	0.9	.041
			54765.09	1.2	.053

Tucana-Horologium members

HD 105	00:05:52.5	-41:45:11	54249.41	2.1	.010
HD 987	00:13:53.0	-74:41:18	54245.42	9.0	.005
HD 1466	00:18:26.1	-63:28:39	54246.42	6.4	.065
			54755.10	5.9	.029
			56087.40	6.3	.041
HIP 1993	00:25:14.7	-61:30:48	56108.39	6.2	.025
			54749.09	6.1	.011
			54251.41	11.8	.013
CD-7824	00:42:20.3	-77:47:40	54755.11	11.0	.011
			54251.40	9.6	.010
			54252.42	8.3	.005
HD 8558	01:23:21.3	-57:28:51	54281.37	5.4	.014
			56108.40	6.2	.009
			54755.16	10.4	.023
HD 9054	01:28:08.7	-52:38:19	54755.15	9.3	.060
			54750.15	9.9	.004
			54251.40	12.8	.011
HD 12039	01:57:49.0	-21:54:05	54749.11	11.8	.006
			54755.13	13.5	.005
			56107.40	13.5	.009
HD 13183	02:07:18.1	-53:11:56	54755.13	13.5	.005
			56107.42	14.1	.011
			54749.13	15.0	.010
CD-60416	02:07:32.2	-59:40:21	56128.42	14.1	.033
			56107.40	16.6	.036
			56116.37	14.4	.016
GSC 08491-01194	02:41:47.3	-52:59:31	56125.34	12.4	.054
			54755.12	12.8	.011
			54251.40	13.5	.009
CD-58553	02:42:33.0	-57:39:37	54749.11	11.8	.006
			54755.13	13.5	.005
			56107.40	13.5	.009
CD-351167	03:19:08.7	-35:07:00	54755.13	13.5	.005
			56107.40	13.5	.009
			54749.13	15.0	.010
CD-461064	03:30:49.1	-45:55:57	56107.42	14.1	.011
			54749.13	15.0	.010
			54281.42	14.1	.033
CD-441173	03:31:55.7	-43:59:14	56107.40	16.6	.036
			56116.37	14.4	.016
			56125.34	12.4	.054
HD 22705	03:36:53.4	-49:57:29	56125.34	12.4	.054
			54308.41	19.1	.050
			54765.12	18.5	.037
HD 24636	03:48:11.5	-74:41:39	56125.39	18.7	.011
			56138.34	19.4	.029
			54749.13	-1.5	.138
BD-12943	04:36:47.1	-12:09:21	56138.35	-2.1	.190
			56139.36		
HD 30051*	04:43:17.2	-23:37:42	56139.36		

ID	RA	DEC	MJD	RV (km s ⁻¹)	$\pm\sigma_{meas.}$
TYC 8083-455-1	04:48:00.7	-50:41:26	56140.36	-2.5	.198
			54772.20	18.8	.013
			56125.40	18.8	.018
BD-191062	04:59:32.0	-19:17:42	54795.05	20.6	.021
			56139.37	20.2	.006
			56140.38	19.5	.014
BD-091108	05:15:36.5	-09:30:51	54892.03	20.3	.025
			56144.40	20.7	.028
			56147.39	21.2	.011
CD-302310	05:18:29.0	-30:01:32	54805.22	20.6	.004
			56138.36	20.4	.011
			56139.37	21.6	.012
TYC 8098-414-1	05:33:25.6	-51:17:13	56138.36	20.0	.021
CD-272520	05:49:06.6	-27:33:56	56139.41	23.4	.020
			56140.40	22.6	.012
HD 47875	06:34:41.0	-69:53:06	54236.97	16.7	.006
GSC 09507-02466 ^a	11:40:16.6	-83:21:00	53453.19	12.6	.005
			56139.03	13.5	.011
HD 202917	21:20:50.0	-53:02:03	54226.35	-1.6	.007
HIP 107345	21:44:30.1	-60:58:39	54765.06	1.5	.007
HD 207575	21:52:09.7	-62:03:09	54765.07	1.3	.124
			56087.40	1.7	.110
			56092.42	1.6	.065
HD 222259N	23:39:39.3	-69:11:40	54243.35	5.6	.012
HD 222259S	23:39:39.5	-69:11:45	54243.35	7.8	.017

TW-Hydrae members

TWA 7	10:42:30.1	-33:40:17	54850.35	11.5	.008
TW Hya	11:01:51.9	-34:42:17	54895.23	11.9	.009
CD-298887	11:09:13.8	-30:01:40	56138.99	10.9	.035
TWA 12	11:21:05.5	-38:45:16	56069.16	11.2	.027
			56097.97	10.5	.034
CD-347390A ^a	11:21:17.2	-34:46:46	54876.36	11.0	.020
			56082.05	10.2	.026
			56137.98	10.6	.028
CD-347390B ^a	11:21:17.4	-34:46:50	54864.36	12.0	.009
			56108.05	10.9	.022
			56137.98	11.3	.016
CD-268632A	11:32:41.2	-26:51:56	56097.98	7.6	.018
TWA 9B	11:48:23.7	-37:28:49	56138.02	11.5	.019
			54895.24	9.6	.005
TWA 9A	11:48:24.2	-37:28:49	56138.01	10.5	.012
			56139.03	11.1	.013
			56138.00	10.8	.077
TWA 23	12:07:27.4	-32:47:00	56139.01	11.0	.055
			54853.37	6.2	.008
			56138.01	7.4	.018
CD-397538	12:15:30.7	-39:48:43	54877.35	9.0	.020
			56111.13	8.2	.022
			56137.99	9.0	.013
TWA 16	12:34:56.4	-45:38:07	54903.14	6.6	.029
			56069.12	6.2	.019
			56109.14	6.1	.034

^(*) No longer classified as a member of association with new RV values.^(a) RV values from a single-component Gaussian fit; see Section B.4 for details on target.

Appendix D: List of SACY association members

Table D.1. Full member list for the SACY associations used in this work.

ID	RA	DEC	V Mag.	X	Y	Z	D	SpT
AB Doradus members								
HD 36705	05 28 44.4	-65 26 47	13.2	1.2	-12.7	-8.3	15.2	M4
AB Dor	05 28 44.8	-65 26 55	6.88	1.2	-12.7	-8.3	15.2	K0
AK Pic	06 38 00.4	-61 32 00	6.27	0.4	-19.2	-9.1	21.3	G2
BD+012447	10 28 55.5	+00 50 28	9.65	-2.0	-4.1	4.9	6.7	M1
V429 Gem	07 23 43.6	+20 24 59	10.00	23.8	-7.7	7.2	26.0	K5
BD-034778	20 04 49.4	-02 39 20	10.24	52.1	42.3	-21.2	70.4	K1
BD-12243	01 20 32.3	-11 28 04	8.43	-8.6	5.4	-32.8	34.3	G9
BD-131328	06 02 21.9	-13 55 33	10.55	29.1	-24.6	-11.7	39.9	K4
CD-262425	05 44 13.4	-26 06 15	10.88	42.4	-51.5	-31.9	73.9	K2
CD-342331	05 35 04.1	-34 17 52	11.76	37.1	-61.2	-41.1	82.5	K4
CD-342676	06 08 33.9	-34 02 55	10.28	35.9	-63.8	-31.2	79.6	G9
CD-352722	06 09 19.2	-35 49 31	11.08	10.1	-19.4	-9.5	23.8	M1
CD-401701	05 02 30.4	-39 59 13	10.64	14.4	-29.6	-25.0	41.3	K4
CD-46644	02 10 55.4	-46 03 59	11.24	-0.8	-30.1	-65.8	72.4	K3
CD-481893	05 36 55.1	-47 57 48	9.81	-5.7	-20.6	-13.3	25.2	K6
CD-571654	07 10 50.6	-57 36 46	10.50	-3.5	-116.0	-42.6	123.6	G2
CD-611439	06 39 50.0	-61 28 42	9.75	0.4	-20.3	-9.4	22.4	K7
CD-8480	07 30 59.5	-84 19 28	9.98	27.9	-55.4	-30.3	69.0	G9
CP-19878	05 39 23.2	-19 33 29	10.51	46.9	-44.3	-29.1	70.8	K1
GSC 08544-01037*	06 47 53.4	-57 13 32	11.50	-6.8	-125.6	-53.4	136.6	K4
HD 139751	15 40 28.4	-18 41 46	10.44	31.4	-5.9	17.4	36.4	K4
HD 152555	16 54 08.1	-04 20 25	7.82	41.5	10.7	18.7	46.8	G0
HD 159911	17 37 46.5	-13 14 47	10.03	44.2	9.8	7.8	45.9	K4
HD 16760	02 42 21.3	+38 37 07	8.70	37.9	26.0	-16.1	48.7	G2
HD 17332A	02 47 27.4	+19 22 19	7.32	25.1	10.6	-19.6	33.6	G1
HD 17332B	02 47 27.2	+19 22 21	8.11	25.1	10.6	-19.6	33.6	G6
HD 178085	19 10 57.9	-60 16 20	8.34	50.6	-22.3	-26.6	61.4	G1
HD 199058	20 54 21.1	+09 02 24	8.62	38.7	58.4	-28.6	75.7	G5
HD 201919	21 13 05.3	-17 29 13	10.64	25.9	16.1	-24.7	39.2	K6
HD 217379	23 00 28.0	-26 18 43	10.45	12.3	6.7	-30.5	33.6	K7
HD 222575	23 41 54.3	-35 58 40	9.39	18.8	-0.8	-60.8	63.6	G8
HD 224228	23 56 10.7	-39 03 08	8.22	6.0	-1.8	-21.1	22.0	K2
HD 24681	03 55 20.4	-01 43 45	9.05	40.6	-7.9	-33.7	53.4	G8
HD 25457	04 02 36.7	-00 16 08	5.38	14.8	-2.8	-11.3	18.8	F6
HD 25953	04 06 41.5	+01 41 02	7.83	44.7	-7.5	-31.6	55.3	F5
HD 293857	05 11 09.7	-04 10 54	9.26	63.9	-29.6	-31.6	77.2	G8
HD 31652	04 57 22.3	-09 08 00	9.98	63.5	-33.9	-40.7	82.7	G8
HD 32981	05 06 27.7	-15 49 30	9.13	56.7	-41.5	-40.9	81.3	F9
HD 33999	05 12 35.8	-34 28 48	9.37	45.7	-72.5	-58.7	103.9	F8
HD 35650	05 24 30.2	-38 58 11	9.05	-6.7	-13.6	-9.8	18.1	K6
WX Col	05 37 12.9	-42 42 56	9.55	24.0	-60.8	-39.5	76.4	G7
TYC 7604-1675-1	05 37 13.2	-42 42 57	10.65	24.0	-60.8	-39.5	76.4	K1
UY Pic	05 36 56.9	-47 57 53	7.84	-5.7	-20.6	-13.3	25.2	K0
HD 45270	06 22 30.9	-60 13 07	6.53	-0.2	-21.2	-10.7	23.7	G1
HD 59169	07 26 17.7	-49 40 51	10.22	16.0	-106.1	-28.9	111.1	G7
HD 64982	07 45 35.6	-79 40 08	8.96	27.4	-68.2	-33.2	80.6	G0
HD 6569	01 06 26.2	-14 17 47	9.50	-8.2	7.2	-46.1	47.4	K1
HD 99827	11 25 17.7	-84 57 16	7.70	42.0	-70.2	-33.8	88.5	F6
HD 16760B	02 42 21.0	+38 37 21	10.21	37.6	25.8	-16.0	48.3	K2
HIP 81084	16 33 41.6	-09 33 12	11.30	27.3	3.2	12.7	30.3	M0
IS Eri	03 09 42.3	-09 34 47	8.48	22.1	-4.4	-29.9	37.4	G0
LO Peg	21 31 01.7	+23 20 07	9.19	6.3	22.4	-8.5	24.8	K4
HD 209952	22 08 14.0	-46 57 40	1.73	18.6	-3.3	-24.6	31.0	B6

ID	RA	DEC	V Mag.	X	Y	Z	D	SpT
HD 17573	02 49 59.0	+27 15 38	3.61	39.7	20.2	-24.3	50.7	B8
HW Cet	03 12 34.3	+09 44 57	10.46	43.9	7.2	-37.0	57.9	K3
HD 20888	03 17 59.1	-66 55 37	6.03	9.4	-38.1	-38.4	54.9	A3
V577 Per	03 33 13.5	+46 15 27	8.26	29.4	17.1	-4.8	34.3	G5
HD 21845B	03 33 14.0	+46 15 19	11.20	29.4	17.1	-4.8	34.3	M0
HIP 17695	03 47 23.3	-01 58 20	11.54	12.2	-2.1	-10.7	16.4	M3
TYC 91-82-1	04 37 51.5	+05 03 08	11.01	77.7	-15.6	-39.7	88.6	K0
TYC 5899-26-1	04 52 24.4	-16 49 22	11.61	10.5	-7.6	-8.6	15.6	M3
CD-561032N	04 53 30.5	-55 51 32	12.10	-0.9	-8.6	-6.9	11.1	M3
CD-561032S	04 53 31.2	-55 51 37	11.16	-0.9	-8.6	-6.9	11.1	M3
HD 38497	05 45 41.3	-14 46 30	9.52	55.2	-45.0	-27.5	76.3	G3
CD-412076	05 48 30.4	-41 27 30	11.56	19.7	-47.6	-28.4	58.8	K6
CD-352749	06 11 55.7	-35 29 13	10.61	23.4	-44.7	-21.3	54.8	K1
GSC 08894-00426	06 25 56.1	-60 03 27	12.32	-0.3	-21.3	-10.6	23.8	M3
CD-472500	06 38 45.5	-47 14 18	10.14	23.3	-94.2	-38.4	104.4	G5
V372 Pup	07 28 51.4	-30 14 49	10.14	-6.9	-14.0	-1.6	15.7	M1
HD 82879	09 28 21.1	-78 15 35	8.99	45.4	-105.3	-40.4	121.6	F6
HD 160934	17 38 39.6	+61 14 16	10.45	-0.1	28.0	17.7	33.1	K7
HD 181869	19 23 53.2	-40 36 57	3.96	51.3	-2.1	-21.9	55.8	B8
GJ 4231	21 52 10.4	+05 37 36	12.11	11.2	22.1	-17.8	30.5	M3
HIP 110526A	22 23 29.1	+32 27 34	11.45	-0.0	14.0	-5.3	15.0	M3
HIP 110526B	22 23 29.1	+32 27 32	11.55	-0.0	14.0	-5.3	15.0	M3
HIP 114066	23 06 04.8	+63 55 34	10.87	-9.0	22.7	1.4	24.5	M1
HIP 115162	23 19 39.6	+42 15 10	8.94	12.7	46.2	-15.1	50.2	G4
Kap Psc	23 26 56.0	+01 15 20	4.95	2.9	26.8	-38.7	47.2	A0
HD 223352	23 48 55.5	-28 07 49	4.59	9.1	4.3	-41.0	42.2	A0
PX Vir	13 03 49.7	-05 09 43	7.69	7.3	-9.1	18.3	21.7	K1
TYC 4779-394-1	05 38 56.6	-06 24 41	10.91	12.7	-66.2	-45.1	81.1	G8
TYC 486-4943-1	19 33 03.8	+03 45 40	11.15	53.0	46.2	-9.3	70.9	K3
TYC 1090-543-1	20 54 28.0	+09 06 07	11.68	38.5	58.2	-28.4	75.3	K4
TYC 7605-1429-1	05 41 14.3	-41 17 59	12.29	36.9	-86.9	-54.9	109.2	K4
TYC 7627-2190-1	06 41 18.5	-38 20 36	11.08	22.9	-54.7	-19.6	62.5	K2
TY Col	05 57 50.8	-38 04 03	9.60	20.1	-41.7	-22.9	51.6	G6
TZ Col	05 52 16.0	-28 39 25	9.08	43.5	-59.7	-34.0	81.3	G3
UX Col	05 28 56.5	-33 28 16	10.57	25.4	-39.8	-28.2	55.0	K4

Argus members

TYC 8561-970-1	07 53 55.5	-57 10 07	11.50	0.6	-138.5	-36.3	143.2	K0
BD-202977	09 39 51.4	-21 34 17	10.22	-21.9	-79.1	34.5	89.0	G9
CD-283434	06 49 45.4	-28 59 17	10.62	-50.9	-84.8	-23.0	101.5	G7
CD-292360	05 34 59.2	-29 54 04	10.53	-34.3	-47.1	-31.8	66.4	K3
CD-395833	09 47 19.9	-40 03 10	10.89	-2.1	-109.4	20.0	111.2	K0
CD-422906	07 01 53.4	-42 27 56	10.64	-26.3	-85.3	-25.8	92.9	K1
CD-433604	07 48 49.8	-43 27 06	11.13	-17.4	-78.8	-12.5	81.7	K4
CD-482972	07 28 22.0	-49 08 38	9.85	-11.9	-75.7	-19.9	79.2	G8
CD-483199	07 47 26.0	-49 02 51	10.56	-12.8	-96.3	-20.2	99.2	G7
CD-529381	20 07 23.8	-51 47 27	10.59	24.5	-5.7	-16.0	29.8	K6
CD-561438	06 11 53.0	-56 19 05	11.32	-9.1	-100.8	-53.0	114.2	K0
CD-572315	08 50 08.1	-57 45 59	10.21	9.2	-105.5	-16.1	107.1	K2
CD-582194	08 39 11.6	-58 34 28	10.18	8.3	-100.0	-18.2	102.0	G5
CD-74673	12 20 34.4	-75 39 29	10.72	25.7	-42.8	-11.4	51.2	K3
CD-75652	13 49 12.9	-75 49 48	9.67	46.9	-63.4	-18.7	81.0	G1
HD 129496	14 46 21.4	-67 46 16	8.78	61.6	-64.9	-11.4	90.2	F7
HD 309851	09 55 58.3	-67 21 22	9.90	31.7	-102.3	-18.9	108.8	G1
HD 61005	07 35 47.5	-32 12 14	8.22	-14.1	-32.2	-3.5	35.3	G8
HD 67945	08 09 38.6	-20 13 50	8.08	-34.8	-60.1	8.5	70.0	F0
AP Col	06 04 52.2	-34 33 36	12.96	-3.7	-6.7	-3.4	8.4	M4

ID	RA	DEC	V Mag.	X	Y	Z	D	SpT
TYC 8568-570-1	08 28 34.6	-52 37 04	10.40	-2.5	-138.2	-19.5	139.6	
TYC 8568-1052-1	08 35 43.7	-53 21 20	12.20	0.5	-137.6	-18.4	138.8	K3
1RXS J083624.5-540101	08 36 24.2	-54 01 06	10.18	2.0	-145.9	-20.3	147.3	G0
PMM 5376	08 37 02.3	-52 46 59	14.30	-0.4	-157.7	-19.7	158.9	
CD-522472	08 38 55.7	-52 57 52	11.04	0.4	-150.4	-18.4	151.5	G2
V365 Vel	08 40 06.2	-53 38 07	10.45	2.1	-152.0	-19.3	153.2	G0
VXR PSPC 18	08 40 18.3	-53 30 29	13.54	1.8	-138.8	-17.4	139.9	K4
HD 74374	08 41 22.7	-53 38 09	9.54	2.3	-143.8	-17.9	144.9	F3
V368 Vel	08 41 57.8	-52 52 14	13.57	0.9	-138.4	-15.9	139.3	K7
HD 74714	08 43 17.9	-52 36 11	9.16	0.7	-154.5	-16.9	155.4	F2
CD-522523	08 43 52.3	-53 14 00	9.76	2.1	-144.4	-16.6	145.4	F5
V377 Vel	08 44 26.2	-52 42 32	11.46	1.4	-169.8	-18.4	170.8	G9
V380 Vel	08 45 39.1	-52 26 00	9.91	1.0	-154.8	-15.9	155.6	F8
PMM 2182	08 45 48.0	-53 25 51	10.22	3.0	-145.9	-16.5	146.9	
CD-621197	09 13 30.3	-62 59 09	10.46	22.1	-114.6	-20.3	118.5	K0
HD 85151A	09 48 43.2	-44 54 08	9.61	2.5	-64.6	7.7	65.1	G7
HD 85151B	09 48 43.4	-44 54 09	10.21	2.5	-64.6	7.7	65.1	G9
CD-65817	09 49 09.0	-65 40 21	10.33	40.1	-143.8	-24.0	151.2	G5
HD 310316	10 49 56.1	-69 51 22	10.82	46.4	-110.5	-19.9	121.5	G8
CP-691432	10 53 51.5	-70 02 16	10.66	61.7	-144.2	-26.1	159.0	G2
CD-427422	12 06 32.9	-42 47 51	10.66	43.4	-96.3	37.0	111.9	K0
HD 145689*	16 17 05.4	-67 56 29	5.95	39.2	-32.4	-11.2	52.1	A6
NY Aps	15 12 23.4	-75 15 16	9.42	32.3	-36.3	-12.9	50.3	G9
VXR PSPC 22a	08 40 49.1	-53 37 45	11.08	2.4	-155.7	-19.6	156.9	G1
ASAS J083655-5308.5	08 36 55.0	-53 08 34	11.51	0.3	-141.2	-18.2	142.4	
TYC 8568-407-1	08 34 20.5	-52 50 05	10.34	-0.9	-150.5	-19.7	151.8	G5
HD 73777	08 37 47.0	-52 52 12	9.66	-0.0	-148.4	-18.4	149.5	F5
VXR PSPC 2b	08 37 55.6	-52 57 11	11.55	0.2	-167.6	-20.9	168.9	G9
CD-52 2467	08 38 22.9	-52 56 48	10.95	0.2	-143.7	-17.8	144.8	
V364 Vel	08 39 53.0	-52 57 57	11.86	0.7	-163.5	-19.7	164.7	K0
V376 Vel	08 44 05.2	-52 53 17	10.85	1.6	-162.1	-18.0	163.1	G3
V379 Vel	08 45 26.9	-52 52 02	12.76	1.6	-137.0	-14.8	137.8	K3
TYC 8568-2261-1	08 37 51.6	-53 45 46	11.35	1.9	-151.2	-20.1	152.5	G8
PMM 686	08 39 22.6	-53 55 06	12.63	2.6	-154.6	-20.4	156.0	
PMM 6974	08 34 18.1	-52 15 58	12.26	-2.1	-143.1	-17.9	144.2	
PMM 6978	08 35 01.2	-52 14 01	12.07	-2.0	-143.2	-17.7	144.3	
TYC 8162-1020-1	08 28 45.6	-52 05 27	10.49	-3.5	-136.7	-18.5	138.0	G6
TYC 8569-3687-1	08 43 00.4	-53 54 08	11.16	3.4	-151.7	-18.8	152.9	G9
PMM 7956	08 29 51.9	-51 40 40	11.62	-4.5	-152.4	-19.7	153.7	
PMM 8415	08 40 16.3	-52 56 29	11.84	0.6	-130.8	-15.6	131.7	G9
TYC 7695-335-1	09 28 54.1	-41 01 19	11.65	-7.9	-147.1	18.8	148.5	K3
TYC 8594-58-1	09 02 03.9	-58 08 50	11.30	15.1	-137.2	-18.6	139.3	G8
TYC 9217-641-1	09 42 47.4	-72 39 50	12.30	50.3	-139.2	-39.0	153.1	K1

 β Pic members

AO Men	06 18 28.2	-72 02 41	9.80	7.5	-33.2	-18.3	38.6	K4
AU Mic	20 45 09.5	-31 20 27	8.73	7.7	1.7	-5.9	9.8	M1
AZ Cap	20 56 02.7	-17 10 54	10.62	34.0	19.9	-27.6	48.1	K6
BD+05378*	02 41 25.9	+05 59 18	10.27	-27.5	7.0	-31.0	42.0	K6
BD-136424	23 32 30.9	-12 15 52	10.54	4.3	10.5	-25.7	28.1	M0
BD-211074A	05 06 49.9	-21 35 09	10.29	-10.5	-9.6	-9.0	16.8	M1
BD-211074B	05 06 49.5	-21 35 04	11.61	-12.8	-11.7	-10.9	20.5	M3
CD-2613904	19 11 44.7	-26 04 09	10.39	74.1	14.8	-21.3	78.5	K4
CD-2711535	17 15 03.6	-27 49 40	11.12	83.5	-4.0	9.1	84.1	K5
CD-547336	17 29 55.1	-54 15 49	9.55	60.8	-26.0	-12.7	67.3	K1
CD-571054	05 00 47.1	-57 15 25	10.00	-1.5	-21.3	-16.3	26.9	M0
CD-641208	18 45 37.0	-64 51 46	9.90	22.8	-12.8	-11.5	28.6	K5

ID	RA	DEC	V Mag.	X	Y	Z	D	SpT
CP-722713	22 42 48.9	-71 42 21	10.60	19.6	-18.9	-24.5	36.6	K7
GJ 3305*	04 37 37.5	-02 29 28	10.68	-24.0	-8.1	-15.0	29.4	M1
GSC 07396-00759	18 14 22.1	-32 46 10	12.78	98.1	-0.5	-12.5	98.9	M1
1RXS J195602.8-320720	19 56 02.9	-32 07 19	14.2	52.3	8.0	-26.8	59.3	M4
1RXS J200136.9-331307	20 01 37.2	-33 13 14	12.55	54.0	7.5	-29.4	61.9	M1
GSC 08056-00482	02 36 51.7	-52 03 04	12.11	0.5	-15.1	-24.4	28.7	M2
GSC 08350-01924	17 29 20.7	-50 14 53	13.47	61.4	-22.1	-10.0	66.0	M3
V343 Nor	15 38 57.5	-57 42 27	7.97	31.0	-22.7	-1.2	38.4	K0
HD 139084B	15 38 56.8	-57 42 19	14.80	31.0	-22.7	-1.2	38.4	M5
HD 14082	02 17 25.3	+28 44 42	6.99	-28.1	19.8	-20.2	39.9	F5
HD 164249	18 03 03.4	-51 38 56	7.01	44.3	-14.7	-11.6	48.1	F6
HD 181327	19 22 58.9	-54 32 17	7.04	44.4	-13.8	-22.9	51.8	F6
HD 191089	20 09 05.2	-26 13 26	7.22	44.5	12.8	-24.4	52.3	F6
HD 199143	20 55 47.7	-17 06 51	7.35	32.3	18.9	-26.2	45.7	F7
HD 29391	04 37 36.1	-02 28 25	5.22	-24.0	-8.1	-15.0	29.4	F0
HIP 10679	02 17 24.7	+28 44 30	7.75	-28.5	20.1	-20.5	40.5	G2
BD+30397B	02 27 28.1	+30 58 41	12.44	-31.0	20.8	-19.5	42.1	M2
AG Tri	02 27 29.3	+30 58 25	10.12	-31.0	20.8	-19.5	42.1	K6
GJ 3322	05 01 58.8	+09 58 59	11.98	-35.6	-6.6	-12.4	38.3	M3
AF Lep	05 27 04.8	-11 54 03	6.56	-20.4	-13.9	-11.0	27.0	F7
Beta Pic	05 47 17.1	-51 03 59	3.77	-3.4	-16.4	-9.9	19.5	A3
V824 Ara	17 17 25.5	-66 57 04	7.23	24.7	-17.4	-8.8	31.5	G7
HD 155555C	17 17 31.3	-66 57 06	12.82	24.7	-17.4	-8.8	31.5	M3
HD 161460	17 48 33.7	-53 06 43	9.61	63.7	-24.1	-15.4	69.8	K0
HD 164249B	18 03 04.1	-51 38 56	12.5	44.3	-14.7	-11.6	48.1	M2
HD 165189*	18 06 49.9	-43 25 31	5.67	40.4	-7.5	-7.9	41.8	A5
HD 168210	18 19 52.2	-29 16 33	8.89	71.8	4.2	-8.4	72.4	G5
HD 172555	18 45 26.9	-64 52 17	4.78	22.8	-12.8	-11.5	28.6	A6
CD-3116041	18 50 44.5	-31 47 47	11.20	50.7	3.5	-12.4	52.3	M0
TYC 6872-1011-1	18 58 04.2	-29 53 05	11.78	74.7	8.4	-19.4	77.6	M0
Eta Tel	19 22 51.2	-54 25 26	5.02	41.4	-12.7	-21.3	48.3	A0
GJ 799 B	20 41 51.1	-32 26 10	11.09	7.5	1.5	-5.6	9.5	M4
AT Mic	20 41 51.2	-32 26 07	10.99	7.5	1.5	-5.6	9.5	M4
TYC 2211-1309-1	22 00 41.6	+27 15 14	11.43	5.7	42.7	-17.3	46.4	M0
PZ Tel	18 53 05.9	-50 10 50	8.29	46.8	-11.5	-18.3	51.5	G9
TWA 22	10 17 26.9	-53 54 27	14.41	-3.5	-17.2	0.7	17.2	M5
TX PsA	22 45 00.0	-33 15 26	13.36	9.2	2.0	-17.9	20.2	M5
TYC 112-917-1	05 20 00.3	+06 13 04	11.58	-62.8	-18.5	-20.2	68.5	K4
TYC 112-1486-1	05 20 31.8	+06 16 11	11.68	-64.0	-18.8	-20.3	69.7	K4
TYC 7443-1102-1	19 56 04.4	-32 07 38	11.55	49.5	7.6	-25.4	56.2	M0
TYC 9073-762-1	18 46 52.6	-62 10 36	12.08	42.4	-21.2	-20.4	51.6	M1
V1005 Ori	04 59 34.8	+01 47 01	10.05	-21.3	-6.8	-9.9	24.5	M0
V1311 Ori*	05 32 04.5	-03 05 29	11.44	-34.5	-17.2	-13.3	40.8	M2
V4046 Sgr	18 14 10.5	-32 47 33	10.94	75.7	-0.4	-9.6	76.3	K6
WW PsA	22 44 58.0	-33 15 02	12.07	9.2	2.0	-17.9	20.2	M4

Carina members

BD-20951	04 52 49.5	-19 55 02	10.00	-46.2	-37.8	-41.4	72.6	K1
CD-423328	07 33 21.2	-42 55 42	11.42	-28.4	-111.9	-22.6	117.6	K1
CD-482324	06 28 06.1	-48 26 53	10.96	-27.4	-117.0	-52.6	131.2	G9
CD-494008	08 57 52.2	-49 41 51	10.51	-1.0	-108.7	-5.0	108.8	G9
CD-542499	08 59 28.7	-54 46 49	10.08	7.2	-117.9	-11.9	118.7	G5
CD-542644	09 13 16.9	-55 29 03	11.36	13.2	-141.3	-11.8	142.4	G5
CD-552543	09 09 29.4	-55 38 27	10.21	11.1	-124.0	-11.5	125.0	G8
CD-571709	07 21 23.7	-57 20 37	10.73	-2.4	-95.1	-32.3	100.5	K0
CD-612010	08 42 00.5	-62 18 26	10.95	18.9	-133.9	-29.3	138.4	K0
CD-75392	08 50 05.4	-75 54 38	10.59	33.9	-93.3	-35.3	105.4	G9

ID	RA	DEC	V Mag.	X	Y	Z	D	SpT
CP-541712	08 37 10.9	-55 18 10	11.04	5.8	-176.1	-26.6	178.2	G9
CP-551885*	09 00 03.4	-55 38 24	10.83	9.2	-124.9	-13.7	126.0	G5
CP-621293	09 43 08.8	-63 13 04	10.44	17.6	-73.5	-10.2	76.3	G7
HD 107722	12 23 29.0	-77 40 51	8.30	33.1	-54.3	-16.9	65.8	F6
HD 189285*	19 59 24.1	-04 32 06	9.52	42.1	31.3	-16.2	54.9	G7
HD 221451*	23 32 19.2	-13 37 18	8.59	7.9	17.1	-44.6	48.4	G8
HD 269620	05 29 27.1	-68 52 05	9.56	13.5	-82.5	-53.3	99.1	G6
HD 309751	09 31 44.7	-65 14 53	11.33	39.1	-157.6	-28.7	164.9	G5
HD 42270	05 53 29.3	-81 56 53	9.14	21.4	-48.1	-29.0	60.1	K0
HD 49855*	06 43 46.2	-71 58 35	9.06	11.5	-50.8	-25.7	58.1	G7
HD 8813	01 23 25.9	-76 36 42	8.37	18.0	-30.5	-30.1	46.5	G6
CD-65149	03 06 14.5	-65 21 32	10.30	15.4	-65.0	-69.9	96.7	K0
HD 19545	03 07 50.8	-27 49 52	6.18	-20.3	-18.5	-47.2	54.6	A3
HD 22213	03 34 16.4	-12 04 07	8.86	-33.1	-11.7	-40.4	53.5	G7
CD-441533	04 22 45.7	-44 32 52	10.47	-24.3	-66.6	-70.1	99.7	K0
HD 269921	05 38 34.5	-68 53 07	10.28	13.8	-84.8	-53.1	101.0	G7
CD-372984	06 39 46.7	-37 50 10	10.90	-29.1	-67.7	-24.5	77.7	K1
CD-521641	06 41 12.5	-52 07 39	10.83	-13.4	-87.4	-36.8	95.8	K0
HD 48097*	06 42 24.3	+17 38 43	5.20	-41.7	-12.1	4.6	43.7	A2
CD-412572	06 45 37.9	-41 12 41	10.74	-24.6	-69.2	-24.6	77.5	K0
HD 51062	06 53 47.4	-43 06 51	9.23	-26.4	-85.9	-28.8	94.4	G5
HIP 38712	07 55 31.4	+08 51 47	5.85	-31.4	-19.7	12.2	39.0	F2
BD-072388	08 13 51.0	-07 38 25	9.32	-28.2	-33.1	11.2	44.9	K1
CD-532515	08 51 56.4	-53 55 57	11.06	4.9	-130.4	-13.9	131.2	G9
HD 83096*	09 31 24.9	-73 44 49	7.49	27.4	-75.2	-23.1	83.3	F2
HIP 46720B*	09 31 25.2	-73 44 51	10.02	27.4	-75.2	-23.1	83.3	G9
CD-484797	09 33 14.3	-48 48 33	11.72	2.6	-52.1	1.9	52.2	K6
CD-69783	10 41 23.0	-69 40 43	10.27	36.4	-90.0	-16.4	98.5	G8
HD 152598	16 52 58.1	+31 42 06	5.34	13.7	18.5	17.9	29.2	F0
TYC 9486-927-1	21 25 27.5	-81 38 28	11.85	21.7	-25.2	-20.9	39.3	M1
BD-035579	23 09 37.1	-02 25 55	10.99	9.4	32.6	-49.0	59.6	K4
HD 221452*	23 32 22.7	-13 39 07	9.20	8.1	17.4	-45.6	49.5	K0
TYC 460-624-1*	18 45 10.3	+06 20 16	10.76	22.0	17.1	2.1	27.9	M1
TYC 8174-1586-1	09 11 15.8	-50 14 15	11.81	2.6	-115.2	-2.8	115.3	K5
TYC 8557-1251-1	07 55 31.6	-54 36 51	11.44	-6.6	-194.1	-45.8	199.5	G9
TYC 8570-1980-1	08 11 09.3	-55 55 56	11.52	0.9	-145.0	-30.8	148.2	G9
TYC 8582-3040-1	08 57 45.6	-54 08 37	11.71	7.0	-140.9	-13.7	141.7	K2
TYC 8590-1193-1	08 56 31.5	-57 00 41	11.83	16.0	-185.8	-24.6	188.1	K0
TYC 8946-872-1*	09 55 15.1	-62 03 32	12.01	42.1	-171.3	-18.3	177.3	K2
TYC 8962-1747-1	11 08 07.9	-63 41 47	12.05	36.3	-90.7	-5.3	97.8	K6
TYC 9217-417-1	09 59 57.7	-72 21 47	11.70	32.2	-85.2	-22.2	93.7	K4

Columbus members

TYC 8862-19-1	02 58 04.0	-62 41 14	11.67	11.9	-58.8	-68.6	91.1	K3
TYC 9178-284-1	06 55 25.2	-68 06 21	11.91	14.1	-92.3	-42.9	102.8	K4
BD-191194	05 30 19.1	-19 16 32	9.62	-80.8	-73.3	-53.7	121.6	G6
BD-04700	03 57 37.2	-04 16 16	10.61	-76.5	-19.3	-66.5	103.2	G8
BD-081195	05 38 35.0	-08 56 40	9.84	-63.8	-41.1	-27.9	80.9	G7
BD-08995	04 58 48.6	-08 43 40	10.32	-67.7	-35.7	-42.3	87.4	K0
BD-11648	03 21 49.7	-10 52 18	11.32	-75.2	-21.0	-96.8	124.4	K0
BD-15705*	04 02 16.5	-15 21 30	10.17	-30.6	-16.4	-33.9	48.5	K3
BD-16351	02 01 35.6	-16 10 01	10.33	-26.9	-1.2	-75.6	80.3	K1
CD-292531	05 50 21.4	-29 15 21	11.31	-58.1	-81.0	-47.1	110.2	K0
CD-361785	04 34 50.8	-35 47 21	10.84	-31.1	-49.6	-53.1	79.0	K1
CD-363202	06 52 46.7	-36 36 17	11.22	-34.2	-78.6	-23.8	89.0	K2
CD-382198	05 45 16.3	-38 36 49	10.95	-51.5	-106.3	-65.0	134.8	G9
CD-392075*	05 37 05.3	-39 32 26	9.52	-18.7	-39.7	-25.9	51.0	K1

ID	RA	DEC	V Mag.	X	Y	Z	D	SpT
CD-393026	07 01 51.8	-39 22 04	11.05	-32.5	-88.5	-25.2	97.6	G9
CD-402458	06 26 06.9	-41 02 54	10.00	-31.9	-83.3	-35.9	96.2	K0
CD-431395	04 21 48.7	-43 17 33	10.18	-35.4	-88.4	-95.0	134.5	G7
CD-44753	02 30 32.4	-43 42 23	10.42	-4.2	-21.7	-45.5	50.6	K5
CD-52381	01 52 14.6	-52 19 33	10.89	8.7	-38.8	-75.8	85.6	K2
CD-544320*	11 45 51.8	-55 20 46	10.24	20.9	-47.7	5.8	52.4	K5
CP-522481	09 32 26.1	-52 37 40	10.86	9.3	-99.2	-1.3	99.6	G8
CP-531875*	08 45 52.7	-53 27 28	10.42	3.2	-151.6	-17.2	152.6	G2
GSC 08077-01788	04 51 53.0	-46 47 31	13.03	-18.1	-57.8	-49.9	78.5	M0
HD 26980	04 14 22.6	-38 19 02	9.08	-26.9	-48.7	-58.4	80.7	G3
HD 272836	04 53 05.2	-48 44 39	10.78	-15.3	-57.7	-48.7	77.0	K2
HD 274561	05 28 55.1	-45 34 58	11.45	-23.2	-69.6	-47.7	87.5	K1
HD 27679	04 21 10.3	-24 32 21	9.43	-41.2	-37.3	-51.9	76.0	G2
HD 298936	10 13 14.8	-52 30 54	9.76	9.6	-54.0	3.1	54.9	K3
HD 31242N	04 51 53.5	-46 47 13	9.85	-15.9	-50.8	-43.9	69.0	G5
HD 32309	05 01 25.6	-20 03 07	4.91	-38.9	-32.9	-32.9	60.6	B9
HD 32372	05 00 51.9	-41 01 07	9.50	-25.2	-54.9	-46.6	76.3	G5
HD 40216	05 55 43.2	-38 06 16	7.46	-21.2	-43.7	-24.4	54.4	F7
AB Pic	06 19 12.9	-58 03 16	9.20	-2.2	-41.0	-20.9	46.1	K1
HD 48370	06 43 01.0	-02 53 19	7.92	-26.9	-18.5	-1.8	32.7	G8
HD 51797	06 56 23.5	-46 46 55	9.84	-16.6	-70.0	-24.2	75.9	K0
HD 55279	07 00 30.5	-79 41 46	10.08	19.3	-49.1	-26.0	58.8	K2
V479 Car	09 23 35.0	-61 11 36	10.16	15.7	-85.5	-11.9	87.7	K1
HD 984	00 14 10.2	-07 11 57	7.32	-2.2	17.4	-43.8	47.2	F5
TYC 119-497-1	05 37 46.5	+02 31 26	11.01	-60.5	-24.4	-17.6	67.6	K5
TYC 119-1242-1	05 37 45.3	+02 30 57	10.96	-61.8	-25.0	-18.0	69.1	K5
TYC 4810-181-1	06 31 55.2	-07 04 59	11.80	-74.4	-56.2	-12.3	94.0	K3
AH Lep	05 34 09.2	-15 17 03	8.41	-44.2	-35.2	-25.0	61.8	G3
BD+03480	03 28 15.0	+04 09 48	9.70	-61.8	0.6	-53.5	81.7	G6
BD+08742	04 42 32.1	+09 06 01	11.02	-96.8	-14.3	-42.2	106.6	K0
BD+443670	21 00 47.0	+45 30 10	8.70	3.4	58.1	-0.5	58.2	G2
CD-441568	04 27 20.5	-44 20 39	10.91	-21.0	-56.5	-57.9	83.6	K1
CD-521363	05 51 01.2	-52 38 13	10.61	-17.0	-99.2	-58.6	116.5	G9
CD-53386	02 01 53.7	-52 34 53	11.74	9.5	-51.8	-96.3	109.8	K2
CD-63408	08 24 06.0	-63 34 03	9.87	14.8	-106.3	-28.0	110.9	G5
GSC 08499-00304	03 24 15.0	-59 01 13	12.09	4.3	-60.2	-68.7	91.4	K6
HD 16754	02 39 48.0	-42 53 30	4.74	-5.1	-20.0	-40.5	45.5	A1
HD 21997	03 31 53.6	-25 36 51	6.38	-32.3	-27.0	-58.3	71.9	A3
HD 222439	23 40 24.5	+44 20 02	4.15	-16.7	46.5	-14.8	51.6	B9
HD 23384	03 47 10.6	+51 42 23	6.90	-48.9	30.1	-2.3	57.5	F3
HD 295290	06 40 22.3	-03 31 59	9.00	-50.0	-34.8	-4.3	61.1	K0
HD 30447	04 46 49.5	-26 18 09	7.85	-43.6	-45.7	-49.2	80.1	F3
HD 31647A	04 59 15.4	+37 53 25	4.99	-51.0	11.6	-2.6	52.4	A0
HD 31647B	04 59 15.4	+37 53 30	8.19	-51.0	11.6	-2.6	52.4	G0
HD 35114	05 20 38.0	-39 45 18	7.34	-17.4	-36.2	-26.8	48.3	F6
HD 35841	05 26 36.6	-22 29 24	8.91	-55.6	-56.1	-42.2	89.6	F3
HD 36329	05 29 24.1	-34 30 56	9.18	-31.6	-51.9	-36.5	70.9	G3
HD 37286	05 36 10.3	-28 42 29	6.26	-28.3	-37.1	-24.9	52.9	A2
HD 37484	05 37 39.6	-28 37 35	7.26	-30.5	-40.0	-26.4	56.8	F4
HD 38206	05 43 21.7	-18 33 27	5.73	-50.8	-46.9	-29.5	75.2	A0
HD 38207	05 43 21.0	-20 11 21	8.46	-64.7	-63.4	-39.7	98.9	F2
HD 38397	05 43 35.8	-39 55 25	8.14	-18.7	-41.1	-25.5	51.9	G0
HD 43989	06 19 08.1	-03 26 20	7.91	-41.1	-26.0	-7.5	49.2	F9
HIP 17248	03 41 37.3	+55 13 07	11.34	-29.3	20.0	0.0	35.5	M0
RT Pic	06 00 41.3	-44 53 50	9.09	-14.6	-44.4	-24.2	52.6	G8
TYC 65-1471-1	03 48 58.8	+01 10 54	11.4	-84.6	-10.0	-68.5	109.3	K3
V342 Peg	23 07 28.7	+21 08 03	5.97	-1.5	32.0	-22.9	39.4	A5
TYC 5900-1180-1*	04 58 35.8	-15 37 31	11.15	-97.2	-68.3	-73.8	139.9	G9

ID	RA	DEC	V Mag.	X	Y	Z	D	SpT
ϵ -Chamaeleon members								
CD-691055	12 58 25.6	-70 28 49	9.97	57.7	-87.1	-14.0	105.4	K0
CD-74712	12 39 21.3	-75 02 39	10.30	55.0	-87.5	-22.3	105.7	K3
CP-681894	13 22 07.5	-69 38 12	10.35	60.9	-85.0	-12.7	105.3	K1
DZ Cha	11 49 31.9	-78 51 01	12.9	46.9	-81.8	-27.7	98.3	M0
EG Cha	08 36 56.2	-78 56 46	11.36	36.7	-89.7	-38.8	104.4	K4
EO Cha	08 44 31.9	-78 46 31	12.53	33.9	-82.5	-35.0	95.8	M0
EQ Cha*	08 47 56.8	-78 54 53	13.92	33.2	-80.1	-33.9	93.1	M2
1RXS J091528.1-760856	09 15 29.1	-76 08 47	12.08	37.9	-98.1	-35.2	110.9	K6
GSC 09239-01495	12 19 43.8	-74 03 57	13.08	52.2	-87.8	-20.5	104.2	M0
GSC 09239-01572	12 20 21.9	-74 07 39	12.85	54.6	-91.7	-21.5	108.9	K7
1RXS J093455.3-780414	09 34 56.1	-78 04 19	14.53	43.3	-100.0	-37.6	115.3	M2
G94010229 ^a	10 05 20.0	-77 48 42	12.75	34.2	-75.0	-26.4	86.6	M1
GSC 09415-02676*	11 58 26.9	-77 54 45	14.29	54.0	-93.2	-29.5	111.7	M3
1RXS J121645.2-775339	12 16 46.0	-77 53 33	13.88	57.7	-95.7	-30.3	115.8	M4
GSC 09420-00948	12 02 03.8	-78 53 01	12.48	51.9	-88.2	-29.8	106.6	M0
DX Cha	12 00 05.1	-78 11 35	6.73	55.7	-95.7	-30.9	115.0	A8
HD 104237-5	12 00 08.3	-78 11 40	14.28	55.7	-95.7	-30.9	115.0	M3
HD 104237-6	12 00 09.3	-78 11 42	12.08	55.7	-95.7	-30.9	115.0	K4
HD 104467	12 01 39.1	-78 59 17	8.56	51.4	-87.3	-29.7	105.6	G3
HD 105923	12 11 38.1	-71 10 36	9.16	56.6	-99.2	-17.2	115.5	G8
HIP 58490	11 59 42.3	-76 01 26	11.31	48.7	-85.3	-23.5	101.0	K4
TYC 9245-535-1	12 56 08.4	-69 26 54	12.06	62.3	-94.7	-13.1	114.1	K7
Eps Cha	11 59 37.6	-78 13 19	5.34	53.8	-92.5	-29.9	111.1	B9
GSC 09416-01029	12 04 36.2	-77 31 35	13.81	55.1	-94.2	-29.0	112.9	M2
HIP 42794	08 43 12.2	-79 04 12	6.80	33.0	-79.5	-34.1	92.6	A7
HIP 58410	11 58 35.2	-77 49 31	6.73	52.5	-90.8	-28.6	108.7	A7
Eta Cha	08 41 19.5	-78 57 48	5.46	33.7	-81.8	-35.1	95.2	B8
T Cha	11 57 13.5	-79 21 32	9.85	50.8	-86.8	-30.3	105.0	K0
Octans members								
BD-201111	05 32 29.3	-20 43 33	10.4	-82.4	-79.4	-56.4	127.6	G7
CD-303394N	06 40 04.9	-30 33 03	9.84	-72.4	-123.7	-40.1	148.8	F6
CD-303394S	06 40 05.7	-30 33 09	10.24	-80.9	-138.2	-44.8	166.3	F9
CD-431451	04 30 27.3	-42 48 47	10.75	-35.7	-85.8	-87.8	127.8	G9
CD-471999	05 43 32.1	-47 41 11	10.19	-38.8	-138.7	-85.9	167.7	G0
CD-492037	06 03 35.4	-49 11 26	11.18	-33.0	-139.5	-75.4	162.0	K0
CD-58860	04 11 55.7	-58 01 47	10.01	-1.5	-74.2	-70.5	102.4	G6
CD-66395	06 25 12.4	-66 29 10	10.92	14.2	-125.8	-65.3	142.4	K0
CD-72248	05 06 50.6	-72 21 12	10.91	32.3	-130.8	-89.5	161.7	K0
CD-87121	23 58 17.7	-86 26 24	9.98	56.3	-83.8	-59.7	117.3	G8
CP-82784	19 53 56.8	-82 40 42	10.87	80.9	-93.2	-68.0	140.9	K1
HD 155177	17 42 09.0	-86 08 05	8.88	76.1	-100.8	-61.4	140.4	F5
HD 274576	05 28 51.4	-46 28 19	10.57	-33.0	-105.3	-72.1	131.8	G6
CP-791037	19 47 03.9	-78 57 43	11.16	107.4	-106.6	-84.7	173.4	G8
TYC 9300-891-1	18 49 48.7	-71 57 10	11.43	125.1	-94.2	-75.0	173.6	K0
TYC 7066-1037-1	05 58 11.8	-35 00 49	11.24	-57.2	-103.1	-56.0	130.5	G9
TYC 9300-529-1	18 49 45.1	-71 56 58	11.59	138.0	-104.0	-82.7	191.6	K0

ID	RA	DEC	V Mag.	X	Y	Z	D	SpT
Tucana Horologium members								
AF Hor	02 41 47.3	-52 59 31	12.21	0.8	-22.4	-34.6	41.2	M2
BD-091108	05 15 36.5	-09 30 51	9.79	-60.1	-35.6	-33.4	77.4	G5
BD-12943	04 36 47.1	-12 09 21	9.86	-49.0	-26.9	-39.6	68.5	K0
BD-191062	04 59 32.0	-19 17 42	10.65	-41.9	-34.2	-35.1	64.5	K3
CD-272520	05 49 06.6	-27 33 56	10.22	-40.4	-52.6	-30.9	73.2	G9
CD-302310	05 18 29.0	-30 01 32	11.66	-34.3	-45.4	-35.7	67.2	K4
CD-351167	03 19 08.7	-35 07 00	11.12	-13.0	-19.5	-36.9	43.7	K7
CD-441173	03 31 55.7	-43 59 14	10.90	-8.4	-24.9	-35.9	44.5	K6
CD-461064	03 30 49.1	-45 55 57	9.55	-6.8	-24.5	-34.2	42.6	K3
CD-58553	02 42 33.0	-57 39 37	10.98	3.9	-28.2	-38.8	48.1	K5
CD-60416	02 07 32.2	-59 40 21	10.68	7.1	-24.4	-36.2	44.2	K5
CD-7824	00 42 20.3	-77 47 40	10.21	21.2	-32.0	-31.4	49.6	K3
HIP 1993	00 25 14.7	-61 30 48	11.47	15.6	-19.7	-36.4	44.2	M0
HD 16978	02 39 35.4	-68 16 01	4.12	10.5	-30.7	-33.4	46.6	B9
HD 105	00 05 52.5	-41 45 11	7.53	10.4	-5.4	-37.6	39.4	G0
HD 12039	01 57 49.0	-21 54 05	8.66	-10.7	-3.4	-39.2	40.8	G4
HD 12894	02 04 35.1	-54 52 54	6.46	5.2	-23.9	-41.1	47.8	F4
HD 13183	02 07 18.1	-53 11 56	8.63	4.3	-24.9	-44.4	51.1	G7
HD 13246	02 07 26.1	-59 40 46	7.50	7.1	-24.4	-36.2	44.2	F7
HD 1466	00 18 26.1	-63 28 39	7.45	15.6	-19.3	-33.3	41.5	F8
HD 17250	02 46 14.6	+05 35 33	7.88	-36.1	8.0	-39.8	54.3	F8
HD 20121AB	03 12 25.8	-44 25 11	6.40	-6.5	-22.3	-35.7	42.6	F5
HD 202917	21 20 50.0	-53 02 03	8.69	29.9	-8.5	-29.6	42.9	G7
HD 20385	03 16 40.7	-03 31 49	7.48	-32.8	-2.9	-36.6	49.2	F5
HD 207575	21 52 09.7	-62 03 09	7.22	28.2	-16.0	-31.6	45.3	F5
HD 207964	21 55 11.4	-61 53 12	6.56	28.7	-16.3	-32.7	46.5	F4
HD 222259S	23 39 39.5	-69 11 45	8.49	21.0	-23.3	-33.2	45.7	G6
HD 222259N	23 39 39.3	-69 11 40	9.84	21.0	-23.3	-33.2	45.7	K3
HD 22705	03 36 53.4	-49 57 29	7.65	-4.6	-26.8	-33.7	43.3	G2
HD 24636	03 48 11.5	-74 41 39	7.13	14.3	-40.4	-32.9	54.0	F3
HD 29615	04 38 43.9	-27 02 02	8.47	-29.6	-31.4	-36.0	56.2	G3
HD 30051*	04 43 17.2	-23 37 42	7.12	-36.8	-34.1	-39.2	63.7	F2
HD 32195	04 48 05.2	-80 46 45	8.14	20.8	-47.6	-31.9	61.0	F7
HD 47875	06 34 41.0	-69 53 06	9.17	11.1	-60.9	-31.2	69.3	G4
HD 8558	01 23 21.3	-57 28 51	8.51	10.6	-23.1	-42.5	49.5	G7
HD 9054	01 28 08.7	-52 38 19	9.07	5.6	-15.0	-32.2	36.0	K1
HD 987	00 13 53.0	-74 41 18	8.78	19.5	-26.5	-29.9	44.5	G8
HIP 107345	21 44 30.1	-60 58 39	11.61	29.0	-15.2	-31.6	45.5	M0
TYC 9344-293-1	23 26 10.7	-73 23 50	11.83	21.8	-25.0	-30.3	44.9	M0
CD-53544	02 41 46.8	-52 59 52	10.22	0.8	-22.4	-34.6	41.2	K6
CD-86147	23 27 49.4	-86 13 19	9.29	28.8	-41.9	-30.1	59.1	G8
ASAS J015220-5950.4	01 52 18.3	-59 50 17	12.57	7.2	-20.5	-31.8	38.5	M2
1RXS J100104.1-791314	10 01 08.8	-79 13 08	13.30	30.5	-64.7	-24.6	75.6	M0
HD 24071	03 48 35.9	-37 37 12	4.79	-15.7	-27.4	-39.7	50.7	A1
HD 25042	04 00 32.0	-41 44 54	8.36	-12.8	-29.2	-36.6	48.5	G3
HD 2884	00 31 32.7	-62 57 30	4.36	14.6	-19.5	-33.6	41.5	B9
HD 2885	00 31 33.5	-62 57 56	4.77	15.0	-20.1	-34.6	42.7	A2
HD 3003	00 32 43.9	-63 01 53	5.07	15.9	-21.5	-36.8	45.5	A0
HD 3221	00 34 51.2	-61 54 58	9.61	14.9	-20.2	-36.0	43.9	K4
HD 53842	06 46 13.5	-83 59 30	7.46	21.9	-44.6	-25.5	55.8	F5
HIP 1910	00 24 09.0	-62 11 04	11.49	16.6	-20.9	-37.6	46.1	M0
HD 86356	09 51 50.7	-79 01 38	10.20	29.5	-64.0	-24.4	74.6	K0
TYC 9507-2466-1*	11 40 16.6	-83 21 00	11.56	35.5	-59.7	-26.4	74.3	K4
TYC 8083-455-1	04 48 00.7	-50 41 26	11.53	-8.9	-40.8	-34.9	54.4	K7
TYC 8098-414-1	05 33 25.6	-51 17 13	11.74	-8.8	-43.0	-28.3	52.2	K7
HD 193924	20 25 38.9	-56 44 06	1.91	42.4	-14.7	-31.7	54.9	B2

ID	RA	DEC	V Mag.	X	Y	Z	D	SpT
TW-Hydrae members								
HD 14228	02 16 30.6	-51 30 43	3.56	2.1	-22.9	-41.2	47.2	B8
TWA 27	12 07 33.4	-39 32 54	19.95	20.1	-45.7	20.7	54.0	M8
CD-337795	11 31 55.3	-34 36 27	12.12	11.6	-43.6	21.5	50.0	M2
TWA 3A	11 10 27.9	-37 31 52	12.57	7.0	-33.7	13.3	36.9	M4
TWA 3B	11 10 27.8	-37 31 53	13.07	7.0	-33.7	13.3	36.9	M4
HD 96819	11 08 44.0	-28 04 50	5.43	5.8	-48.0	27.4	55.6	A1
HD 98800	11 22 05.3	-24 46 40	9.42	5.5	-37.3	25.2	45.3	K5
TWA 11A	12 36 01.0	-39 52 10	5.78	33.3	-58.4	28.4	73.0	A0
TWA 11B	12 36 00.6	-39 52 16	12.8	31.5	-55.2	26.8	69.0	M2
TWA 26	11 39 51.1	-31 59 21	20.5	10.0	-35.6	20.0	42.0	M8
TWA 5B	11 31 55.4	-34 36 29	20.4	11.6	-43.6	21.5	50.0	M8
TW Hya	11 01 51.9	-34 42 17	11.07	7.7	-50.4	21.6	55.4	K6
TWA 10	12 35 04.2	-41 36 39	12.96	26.7	-46.9	20.9	57.9	M2
TWA 12	11 21 05.5	-38 45 16	12.85	14.7	-58.1	22.8	64.1	M1
CD-347390A*	11 21 17.2	-34 46 46	11.46	11.5	-51.0	23.9	57.5	M1
CD-347390B*	11 21 17.4	-34 46 50	11.96	11.5	-51.0	23.9	57.5	M1
TWA 14	11 13 26.5	-45 23 43	12.8	24.9	-89.9	23.5	96.2	M0
TWA 16	12 34 56.4	-45 38 07	12.8	37.2	-64.7	23.0	78.1	M1
CD-298887	11 09 13.8	-30 01 40	11.43	5.7	-40.7	21.7	46.5	M2
TWA 23	12 07 27.4	-32 47 00	12.67	17.9	-43.4	26.2	53.8	M3
CD-397538	12 15 30.7	-39 48 43	11.44	21.5	-45.1	20.7	54.1	M1
TWA 7	10 42 30.1	-33 40 17	11.65	2.3	-29.9	12.1	32.3	M2
CD-268632A	11 32 41.2	-26 51 56	12.23	7.9	-37.1	24.4	45.1	M3
TWA 8B	11 32 41.2	-26 52 09	15.3	7.7	-36.3	23.9	44.1	M5
TWA 9A	11 48 24.2	-37 28 49	11.26	22.2	-63.3	29.5	73.3	M1
TWA 9B	11 48 23.7	-37 28 49	14.0	22.2	-63.3	29.5	73.3	M1

Notes. (*) No longer classified as a member of association with new RV values. (a) No SIMBAD entry within 5 arcseconds.